FUNCTIONAL NEAR INFRARED SPECTROSCOPY FOR THE ASSESSMENT OF MOTOR CORTEX PLASTICITY IN PEDIATRIC SUBJECTS AFFECTED BY CEREBRAL PALSY

by

BILAL KHAN

Presented to the Faculty of the Graduate School of

The University of Texas at Arlington in Partial Fulfillment

of the Requirements

for the Degree of

MASTER OF SCIENCE IN BIOMEDICAL ENGINEERING

THE UNIVERSITY OF TEXAS AT ARLINGTON

August 2009

ACKNOWLEDGEMENTS

I would like to thank Dr. George Alexandrakis for giving me this great opportunity in pursuing my interests in biomedical engineering. His continuous advice and support have been a great help throughout my research.

I am sincerely grateful to Dr. Khosrow Behbehani for his time and advice on both my project and schoolwork. I would like to also thank Dr. Hanli Liu for her support and suggestions throughout this project. I would also like to show my gratitude to Dr. Delgado for his suggestions of the clinical applications, and for letting me use the new wireless surface EMGs. I am also grateful to Dr. Mario Romero for his advice on the statistical analysis and physiology.

I would like to thank Dr. Fenghua Tian for his advice and suggestions in the technical aspects of this project. I would like to acknowledge Mr. Sameer Dhamne, Mr. Tamer Desouky, and Mr. Nayan Asanini for their help. I would like to also acknowledge Texas Scottish Rite Hospital, Mrs. Nancy Clegg, and the nursing staff for their support throughout this project.

As for my family, I would like to thank my mother, Rubina Khan, for always being there and for her love and support. I would like to also thank my father, Aslam Khan, for his support and advice throughout my life. And of course, there is my brother, Hamza Khan, who never fails to make me laugh. I would like to also thank my lovely fiancé, Sana Muntajibuddin, for her love and support, and for making sure I remembered the circle of Willis. My family members are the most valuable people to me. Without their support, I could not have gone this far. Jazak Allahu Khair.

June 17, 2009

ABSTRACT

FUNCTIONAL NEAR INFRARED SPECTROSCOPY FOR THE ASSESSMENT OF MOTOR CORTEX PLASTICITY IN PEDIATRIC SUBJECTS AFFECTED BY CEREBRAL PALSY

Bilal Khan, M.S.

The University of Texas at Arlington, 2009

Supervising Professor: George Alexandrakis

Functional near infrared spectroscopy (fNIRS) is widely used to monitor hemodynamic changes occurring in the cerebral cortex as a result of neuronal activation. One of the current challenges in this field is that activation-related hemodynamic signals are often eclipsed by global hemodynamic fluctuations due to cardiac pulsation, respiration and Mayer waves. In this study, we demonstrate by using a combination of principal component analysis (PCA) and adaptive filtering that the global hemodynamic modulation signals can be effectively removed from the fNIRS measuring cortical hemodynamic response. While pediatric subjects were performing a finger tapping task, we concurrently recorded cardiac pulsation and respiration using a pulse oximeter and a piezo-electric transducer, respectively. The results indicate that fNIRS data quality is significantly improved, as quantified by temporal signal-to-noise ratio (SNR), contrast-to-noise ratio (CNR), and image SNR metrics after reducing the effects of physiological artifacts. The significant improvement in SNR ($p < 0.0001$), CNR ($p < 0.0001$), and image SNR ($p = 0.0014$) leads to the conclusion that concurrent hemodynamic, cardiac

pulsation, and respiration signal acquisition and filtering methods may need to become standard procedure in fNIRS, neuroimaging protocols.

The filtered data can potentially be used to differentiate between motor cortex activation patterns in normal children and ones affected by cerebral palsy. The ratios of duration over time-to-peak temporal metrics were found to be significantly different ($p < 0.0001$) between normal subjects (1.28 +/- 0.23) and cerebral palsy subjects tapping with their affected hand (0.68 +/- 0.09). In the time-averaged reconstructed images, the distance of activation areas from the middle of the motor cortex in the ipsilateral hemisphere of the tapping hand were also found to be significantly different ($p < 0.0001$) between normal subjects (7.70 cm +/- 1.34 cm) and cerebral palsy subjects (3.50 cm +/- 1.78 cm). Differences were also found in the areas of activation, when taking the difference between the areas of activation in the middle of the motor cortex from the areas of activation in the contralateral hemisphere of the tapping hand. Areas were found which did not have activation according to the time-averaged reconstructed images, but had similar temporal responses as that of the activation area. Images were produced to show these areas of similarity. The same metrics used for the time-averaged images were also found for the similarity images. The distance from center of the similar areas in the ipsilateral hemisphere of the tapping hand were found to be significantly different ($p < 0.0001$) between normal subjects (6.20 cm +/- 2.35 cm) and cerebral palsy subjects (0.50 cm +/- 1.27 cm). The distance from center of similar areas in the controlateral hemisphere of the tapping hand were also found to be significantly different ($p = 0.0183$) between normal subjects (3.10 cm +/- 1.45 cm) and cerebral palsy subjects (1.00 cm +/- 2.11 cm). A significant difference ($p = 0.0110$) was also observed between normal subjects (13.57 cm^2 +/- 5.72 cm^2) and cerebral palsy subjects (3.00 cm^2 +/- 10.30 cm^2) in the areas of similarity, when taking the difference between the areas of similarity in the middle of the motor cortex from the areas of similarity in the controlateral hemisphere of tapping.

The significant difference between normal and cerebral palsy subjects of these temporal and spatial metrics show that fNIRS can be used in the assessment of plasticity of the motor cortex in cerebral palsy patients. These temporal and image metrics can potentially be used as biomarkers to help assess treatment and improvement of CP patients in future studies. These can also be correlated with current cerebral palsy classification schemes, and further improve the sensitivity of current classification schemes.

TABLE OF CONTENTS

ACKNOWLEDGEMENTS iii

ABSTRACT iv

LIST OF ILLUSTRATIONS ix

LIST OF TABLES xi

Chapter Page

1. INTRODUCTION 1

1.1 Principles of Near Infrared Spectroscopy 1

1.1.1 Diffuse Optical Imaging 1

1.1.2 Optical Window 2

1.1.3 Modified Beer-Lambert Law 4

1.2 Brain Physiology 5

1.2.1 Neurovascular Coupling 6

1.2.2 Motor Cortex 8

1.2.3 Pyramidal System 10

1.3 Previous Methods of Filtering fNIRS 11

1.4 Cerebral Palsy (CP) 12

1.5 Study Overview 13

2. MATERIALS AND METHODS 16

2.1 Subjects 16

2.2 Methods of Evaluation Hemiparesis 17

2.2.1 Manual Ability Classification System (MACS) 18

2.2.2 Shriners Hospital for Children Upper Extremity Evaluation (SHUEE) 20

2.3 Measurements 21
2.4 Protocol 23
2.5 Signal and Image Processing 24
2.6 Baseline Correction 26
2.7 Delay Correction 26
2.8 Adaptive Filtering 28
2.9 Averaging 31
3. RESULTS OF FILTERING 32
3.1 Temporal Signal-to-Noise Ratio 32
3.2 Contrast-to-Noise Ratio 36
3.3 Signal-to-Noise Ratio for Reconstructed Images 40
4. DIFFERENCES BETWEEN NORMAL AND CEREBRAL PALSY SUBJECTS 46
4.1 Time-to-Peak and Duration of the Temporal Signals 46
4.2 Time-to-Peak and Duration of the Reconstructed Images 49
4.3 Activation Distance from the Center of the Motor Cortex 52
4.4 Area of Activation of the Reconstructed Images 56
4.5 Similarity of Activation of the Reconstructed Images 59
5. CONCLUSION AND FUTURE WORK 69
5.1 Conclusion 69
5.2 Future Work 72
APPENDIX
A. CW-5 Specifications 74
B. Code for Filtering, Temporal Metrics, and Spatial Metrics 76
REFERENCES 92
BIOGRAPHICAL INFORMATION 98

LIST OF ILLUSTRATIONS

Figure Page

1.1 Electromagnetic Spectrum 1

1.2 Absorption Spectra of HbO, Hb, and Water 3

1.3 Banana-Shaped path of photons when introduced at the scalp....4

1.4 Neurovascular Coupling 8

1.5 Brain Anatomy 9

1.6 Humunculus....9

1.7 Pyramidal System....10

2.1 The geometry of NIRS probes on the motor cortex. The circles represent sources and the squares represent detectors....22

2.2 Overall Instrumentation Setup 23

2.3 (a) Cross-correlation of the pulse oximeter signal to the fNIRS cardiac pulsation frequency range signal. (b) Cross-correlation of the respiration belt signal to the fNIRS respiration frequency range signal. Since the sampling frequency was at 20Hz, each sample represents 0.05s 27

2.4 Flowchart of the Signal Processing Algorithm....30

3.1 The SNR of active channels, before and after filtering, results are for Subject 1 (normal subject) tapping with right finger tapping. Channels 1 to 14 were located on the left hemisphere, and channels 15 to 28 on the right hemisphere of the motor cortex For Subject 1 channels 6, 7, 9, and 10 were the only ones with activation....35

3.2 The SNR of active channels, before and after filtering, results are for Subject 10 (cerebral palsy subject) tapping with left finger tapping. Channel placement as in Figure 3.1, above. For Subject 10 the channels shown were the only ones with activation 35

3.3 Temporal signal averaged over 10 tapping-rest cycles before (thin curve) and after (thick curve) filtering. The encircled area indicates where activation is seen after filtering 36

3.4 Percent change in time-averaged CNR over the length of each experiment. Subjects 1 to 5 were normal subjects and Subjects 6 to 10 were subjects

with cerebral palsy 38

3.5 Percent change in image SNR after filtering.
Subjects 1 to 5 were normal subjects and Subjects 6 to 10 were subjects
with cerebral palsy 42

3.6 Averaged HbO images for Subject 1 (a) before and (b) after filtering.
Notice the deactivation represented in both hemispheres when the
signals are not filtered. After filtering, an activation area is seen in the
left hemisphere 43

4.1 Bar graph presenting the ratio of duration over time-to-peak metrics
For both right finger (right column) and left finger tapping (left column).
Subjects 1 to 5 were normal subjects, Subjects 6 to 8 were right
hemiparesis cerebral palsy subjects, and Subjects 9 and 10 were
left hemiparesis cerebral palsy subjects. 47

4.2 Bar graph presenting the ratio of duration over time-to-peak metrics
for both right finger (right column) and left finger tapping (left column).
for the reconstructed images.Subjects 1 to 5 were normal subjects,
Subjects 6 to 8 were right hemiparesis cerebral palsy subjects,
and Subjects 9 and 10 were left hemiparesis cerebral palsy subjects. 50

4.3 Distance from center measurements of the time-averaged images for left
finger tapping and right finger tapping of normal and CP subjects 54

4.4 Image of the three areas measured. The red area is the left 7 cm of the
left hemisphere, the blue area is the middle 6 cm of the motor cortex
and the green area is the right 7 cm of the right hemisphere 57

4.5 Difference of the middle area of the motor cortex to the contralateral
hemisphere of tapping of the averaged images 58

4.6 Block Diagram of the Similarity Algorithm 61

4.7 Images of a normal subject, Subject 2 left finger tapping, of
(a) average change in HbO concentration
(b) thresholded image showing only the area of activation
and, (c) the similarity image 62

4.8 Images of a cerebral palsy subject, Subject 7 left finger tapping, of
(a) average change in HbO concentration
(b) thresholded image showing only the area of activation
and, (c) the similarity image 63

4.9 Distance from the center measurements of the similarity images
for (a) left finger tapping and for (b) right finger tapping 64

4.10 Difference of the middle area of the motor cortex to the contralateral
hemisphere of tapping of the similarity images 67

LIST OF TABLES

Table Page

2.1 Summary of subjects 17

2.2 Description of each MACS level 19

3.1 One Sampled paired t-Test for SNR....33

3.2 One Sampled paired t-Test for SNR of only normal subjects 34

3.3 One Sampled paired t-Test for SNR of only CP subjects....34

3.4 One Sampled paired t-Test for net CNR 39

3.5 One Sampled paired t-Test for net CNR of only normal subjects 40

3.6 One Sampled paired t-Test for net CNR of only CP subjects 40

3.7 Wilcoxon Signed-Rank test for image SNR....44

3.8 One Sampled paired t-Test for image SNR of only normal subjects....45

3.9 Wilcoxon Signed-Rank test for image SNR of only CP subjects....45

4.1 Two sampled t-Test for the ratio of duration to time-to-peak between normal subjects left finger tapping and right finger tapping 48

4.2 Two sampled t-Test for the ratio of duration to time-to-peak between normal and CP subjects....49

4.3 Two sampled t-Test for the ratio of duration to time-to-peak between normal subjects left finger tapping and right finger tapping from images....51

4.4 Two sampled t-Test for the ratio of duration to time-to-peak between normal and CP subjects from images....52

4.5 Two sampled t-Test for distance to center of the ipsilateral hemisphere of tapping from the averaged images....55

4.6 Two sampled t-Test for distance to center of the contralateral hemisphere of tapping from the averaged images....56

4.7 Two sampled t-Test for area difference from the averaged images....59

4.8 Two sampled t-Test for distance to center of the ipsilateral hemisphere of tapping from the similarity images 65

4.9 Two sampled t-Test for distance to center of the contralateral hemisphere of tapping from the similarity images 66

4.10 Two sampled t-Test for area difference from the similarity images 68

5.1 Summary of Results of Differences between Normal and CP Subjects 71

CHAPTER 1

INTRODUCTION

1.1 Principles of Near Infrared Spectroscopy

1.1.1 Diffuse Optical Imaging

Diffuse optical imaging (DOI) uses the interaction of light, from near-infrared wavelengths with biological tissues, primarily by absorption and elastic scattering. Near-infrared light is an electromagnetic wave in the region of 700nm to 900nm, which are slightly beyond what the human eye can see, as shown in Figure 1.1. There are many physiological molecules which have characteristic absorption within these wavelengths, particularly oxygenated hemoglobin (HbO) and deoxygenated hemoglobin (Hb). The difference in the near-infrared absorption spectra of HbO and Hb allows the separate measurement of the concentrations of these two species [1].

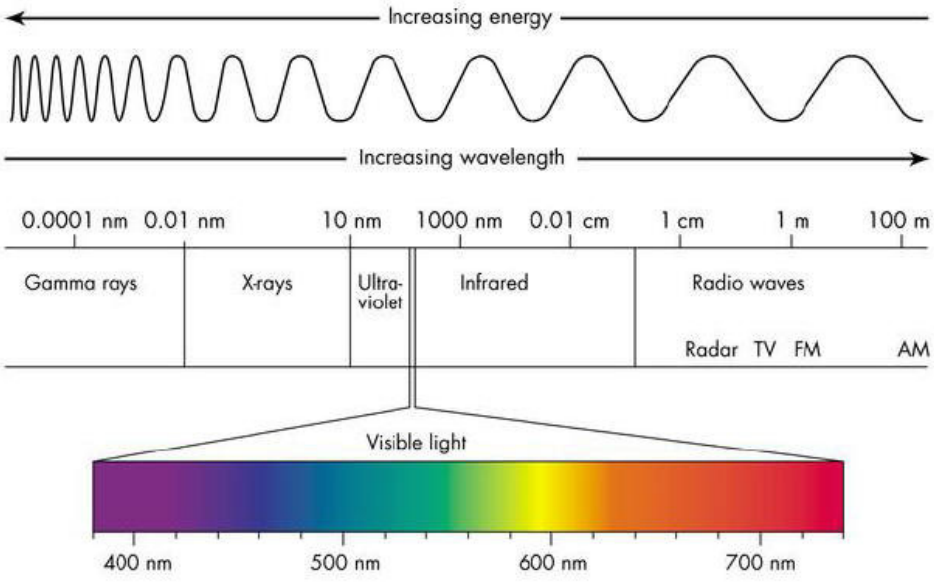

Figure 1.1 Electromagnetic Spectrum

Hemoglobin concentrations can act as an indicator of changes in blood volume and oxygenation of tissues of interest [1], [2]. There are two parameters that describe the interaction between light and the biological tissue; the absorption coefficient, μ_a, and the scattering coefficient, μ_s'. The number of absorption events occurring per unit length is defined by μ_a, and the number scattering events occurring per unit length is defined by μ_s'. In tissue, μ_s' is considerably larger, thus the signals measured at a few millimeters or more are dominated by diffuse light.

Monitoring techniques such as, pulse oximetry and near-infrared spectroscopy (NIRS), take advantage of the different absorption spectra of HbO and Hb. DOI is a spectroscopic method capable of non-invasively measuring concentration changes of HbO and Hb using near-infrared light. These absorption changes are measured by a spatially distributed array of light source-detector pairs with overlapping measurement volumes. The main aim of this method is to process this information further to produce spatially resolved images. These images may display the specific absorption and scattering properties of the tissue, or physiological parameters such as blood volume and oxygenation, or HbO and Hb concentrations [3].

Functional optical brain imaging has faster sampling rates of up to 50 Hz [4], in order to better filter physiological artifacts. It is also better to cover large areas of the brain; where spatial coverage is not limited to the activation area, but also including areas that are not involved with the stimulation. Such spatial coverage improves contrast between regions of activation and its surroundings [5].

1.1.2 Optical Window

Light absorption in tissue occurs due to excitation of atoms or molecules to higher energy states by photons, which get destroyed in the process. μ_a varies at different wavelengths of light for a given material. This variation of μ_a gives the absorption spectrum for that material.

HbO and Hb are the main absorbers in tissue which are strongly linked to tissue oxygenation and metabolism [6]. The absorption spectra for HbO, Hb, and water are shown in Figure 1.2.

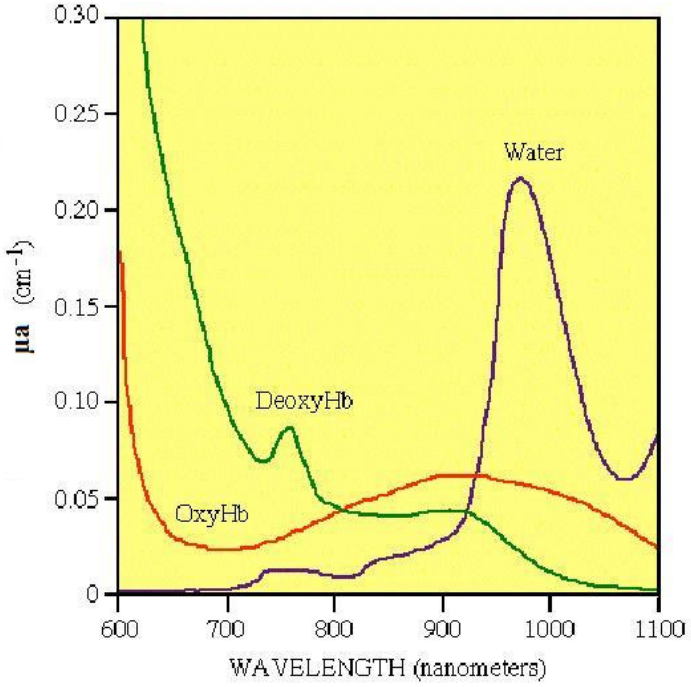

Figure 1.2 Absorption Spectra of HbO, Hb, and Water [1]

Most biological tissues are relatively transparent to light in the near-infrared range between 700 to 900 nm which is usually called the “optical window”. In this window, light is able to propagate through tissue thickness of up to 15 cm for brain, breast, and limbs [6]. At longer wavelengths the absorption of water increases steeply, while at lower wavelengths the absorption increase for both HbO and Hb blocking all light transmission within a few millimeters. Since the absorption spectra of HbO and Hb are significantly different from each other within the "optical window", spectroscopic separation of these compounds is possible using a few sample wavelengths. Thus, the changes of HbO, Hb, and total hemoglobin (HbT) can be measured simultaneously. Since a relatively predictable quantity of photons follows a banana-shaped path when light is emitted from the scalp, these photons can be measured at the scalp with a photodetector as shown in Figure 1.3 [1].

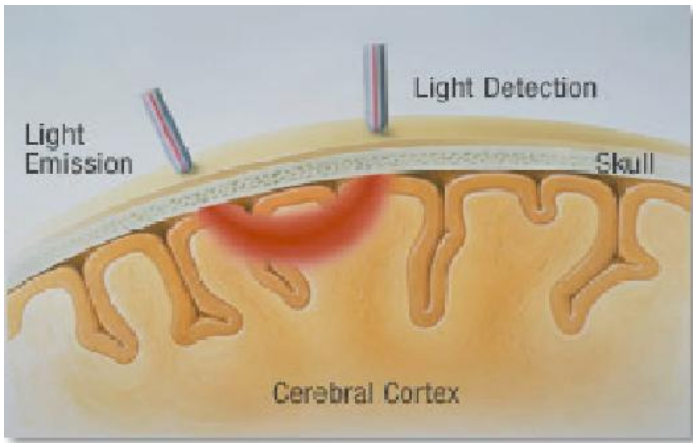

Figure 1.3 Banana-Shaped path of photons when introduced at the scalp [1]

1.1.3 Modified Beer-Lambert Law

In the fNIRS studies, optical absorption causes changes in optical density, which is assumed to be small, and can be modeled as a linear combination of changes in HbO and Hb as given by the modified Beer-Lambert law (MBLL). The MBLL is an empirical description of optical attenuation in a highly scattering medium. Whenever there is a change in the concentration of an absorbing species, the detected light intensity also changes [2], [6]. According the MBLL this concentration change can be measured by the light intensity as shown in equation (1.1)

$$OD = \log(I_o/I) = \epsilon c L = kc \quad \textbf{(1.1)}$$

where OD is the attenuation measured in optical densities, Io is the light intensity before the change of concentration, I is the light intensity after the change of concentration, c is the concentration of the absorbing species, ϵ is the extinction coefficient of the absorbing species, and L is the path length through the tissue. The path length through the tissue can be decomposed into the source-detector separation (d) and the differential path length (DPF),

where L = d * DPF. The differential path length is either measured for a time-domain or frequency-domain measurements, or estimated when using continuous-wave measurements. The source-detector separation can be measured from the probe geometry. The extinction coefficient of the absorbing species, which can be looked up in literature, and the path length the scattered light traveled through the tissue are two pieces that are contained in the proportionality constant, $k = \epsilon * L$.

In order to determine the contribution of multiple chromophores, such as HbO and Hb, one must take measurements at one or more wavelengths per chromophore to be resolved. For example, by measuring the change in light intensity at two wavelengths, and using the known extinction coefficients of HbO (εHbO) and Hb (εHb) at wavelengths within the "optical window", one can then separately determine the concentration changes of HbO and Hb by solving the two equations with two unknowns for Δ[Hb] and Δ[HbO] as shown in equations (1.2), (1.3), and (1.4), where OD_λ is the optical density at wavelength λ, εHbO_λ is the extinction coefficient of HbO at wavelength λ, and εHb_λ is the extinction coefficient of Hb at wavelength λ [2], [6], [7], [8].

$$\Delta[HbO] = (\varepsilon Hb_{\lambda 2} * OD_{\lambda 1} - \varepsilon Hb_{\lambda 1} * OD_{\lambda 2}) / (L*(\varepsilon Hb_{\lambda 2} * \varepsilon HbO_{\lambda 1} - \varepsilon Hb_{\lambda 1} * \varepsilon HbO_{\lambda 2})) \quad \textbf{(1.2)}$$

$$\Delta[Hb] = (\varepsilon HbO_{\lambda 2} * OD_{\lambda 1} - \varepsilon HbO_{\lambda 1} * OD_{\lambda 2}) / (L*(\varepsilon Hb_{\lambda 1} * \varepsilon HbO_{\lambda 2} - \varepsilon Hb_{\lambda 2} * \varepsilon HbO_{\lambda 1})) \quad \textbf{(1.3)}$$

$$\Delta[HbT] = \Delta[Hb] + \Delta[HbO] \quad \textbf{(1.4)}$$

1.2 Brain Physiology

The human brain undergoes many physiological changes as it responds to external stimuli. The influx of oxygenated blood into areas of activation usually over-compensates for the increased demand for oxygen by neurons, which then results in an overabundance of oxygenated blood in these areas [2], [8] - [10]. The change in concentration of deoxygenated and oxygenated hemoglobin secondary to neuronal activity, known as neurovascular coupling,

can be detected using functional near infrared spectroscopy (fNIRS) by detecting the changes in scattering and absorption of near infrared light [11].

1.2.1 Neurovascular Coupling

In the brain, large cerebral arteries, coming from the circle of Willis, branch out into smaller pial arteries and arterioles. The pial arteries travel along the subarachnoid space and branch out into arteries and arterioles which penetrate into the brain. These penetrating arteries and arterioles consist of an endothelial cell layer, a smooth muscle cell layer, and an outer layer consisting of collagen, fibroblasts, and perivascular nerves [12]. Penetrating vessels are separated from the brain by the Virchow-Robin space which consists of cerebral spinal fluid. As the vessels penetrate deeper into the brain the Virchow-Robin space disappears and the vascular basement membrane comes into direct contact with astrocytic end feet. These capillaries consist of endothelial cells, pericytes, and the capillary basal lamina on which astrocytic feet are attached [12]–[14]. The endothelial cells play an important role in the regularization of vascular tone by releasing potent vasoactive factors [12].

Neurovascular coupling is caused by the close interaction between neurons, astrocytes, and vascular cells. The mechanisms underlying neurovascular coupling include ions, metabolic by-products, vasoactive neurotransmitters, and vasoactive factors released in response to neurotransmitters [12]–[14]. Under normal conditions or at resting state the brain relies almost exclusively on glucose oxidation [14]–[17]. A physiological increase of neuronal activity caused by voluntary movement increases cerebral metabolic rates for oxygen and glucose, and increases cerebral blood flow [18]–[20]. The brain has little energy reserves and depends on a continuous supply of glucose and oxygen through cerebral blood flow [12], [16]. As neurons depolorize, the dendrites release neurotransmitters such as glutamate and GABA [12], [16], [21]. Glutamate is responsible for the majority of the synaptic transmission within the cerebral cortex [16], [17], [21]. The uptake of glutamate from the synaptic cleft by astrocytes stimulates

aerobic glycolysis in the astrocytes. For the uptake of every three Na^+ and one glutamate molecule, one glucose molecule also enters the astrocyte. Neurons, unlike astrocytes, cannot uptake glucose, thus neurons depend on astrocytes for glucose uptake [16]. The glycolytic processing of a glucose molecule in the astrocyte results in two lactate molecules which are taken in by a neuron and converted into ATP with the presence of oxygen [20]. Vasoactive factors released in response to neurotransmitters can also cause vasodilation, such as the activation of glutamate receptors. In this case, intracellular Ca^{2+} of astrocytes, associated with glutamate receptor activation, causes Ca^{2+}-dependent enzymes to produce vasodilators, such as nitric oxide (NO) [12], [13]. With increased neuronal activity there is an increase of glutamate release, thus causing an increase of cerebral blood flow, glucose uptake by astrocytes, and glucose availability for astrocyte uptake. Increased blood flow and volume can also be caused by ions, K^+ and H^+, which are generated by the extracellular ionic currents caused by action potentials and synaptic transmissions, causing the smooth muscles in arterioles to hyperpolarize and relax. Increased blood flow can also be caused by neurotransmitters, such as acytelcholine released by active neurons, which cause the smooth muscles in arterioles to relax [12], [13]. With the increase of cerebral blood flow there is also an increase of oxygen availability. With the increased uptake of glucose and availability of oxygen, neurons are able to produce more ATP giving them more energy during stimulation. Surrounding capillaries deliver HbO which releases its oxygen and takes away the CO_2, thus converting it to Hb.

In summary (Figure 1.4), brain activity is associated with a number of physiological events. Neuronal activity is fueled by glucose metabolism, thus increases in neuronal activity increase glucose and oxygen consumption. The reduction of glucose and oxygen in the capillary bed stimulates the brain to increase local arteriolar vasodilation. The arteries dilating results in an increase of local cerebral blood flow and cerebral blood volume, which is a mechanism known as neurovascular coupling.

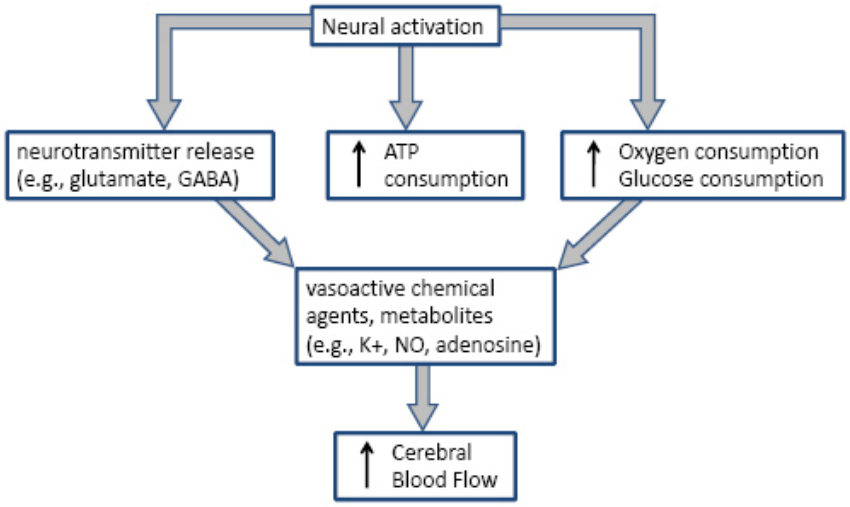

Figure 1.4 Neurovascular Coupling [22]

1.2.2 Motor Cortex

The motor cortex is in the cerebral cortex region of the brain just anterior to the central sulcus. The anatomy of the human brain is shown in Figure 1.5. The motor cortex is involved in planning, control, and execution of voluntary activities [23]. The primary motor cortex (M1) is responsible for sending neuronal impulses controlling movement. It also sends impulses to the lower areas of the body via the spinal cord, and works along with the pre-motor cortex to plan the execution of actions.

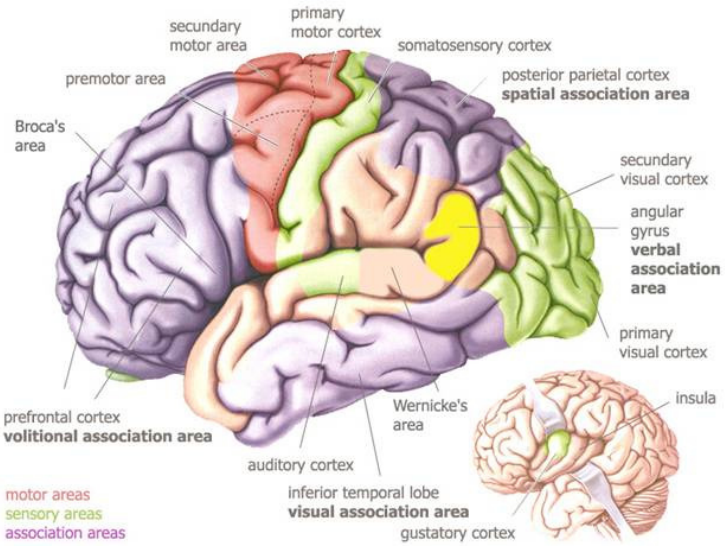

Figure 1.5 Brain Anatomy [24]

The lateral area of the primary motor cortex is divided up into regions for movement of different body parts. Disproportionately large regions in the maps of M1, known as the Humunculus, are devoted to the body parts involved in the most elaborate and complex movements. Thus, movements of specific body parts are devoted to a specific region in the motor cortex [23]. This division is shown in Figure 1.6.

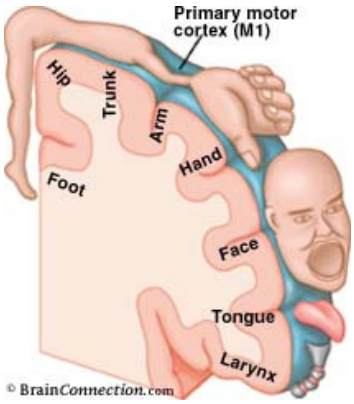

Figure 1.6 Humunculus [25]

1.2.3 Pyramidal System

The pyramidal system, presented in the Figure 1.7, consists of neuronal cell bodies and axons which pass from the cerebral cortex through the brainstem to the spinal cord. In the medulla the pyramidal tract from the right hemisphere crosses the midline to innervate the left spinal cord, and vice versa. Since the pyramidal tract crosses the midline in the medulla, the right hemisphere controls the left side of the body, while the left hemisphere controls the right side of the body. Many of the axons of the pyramidal tract originate from the M1 region of the brain, thus the left hemisphere of the motor cortex controls the right hand, and the left hemisphere controls the right hand [26].

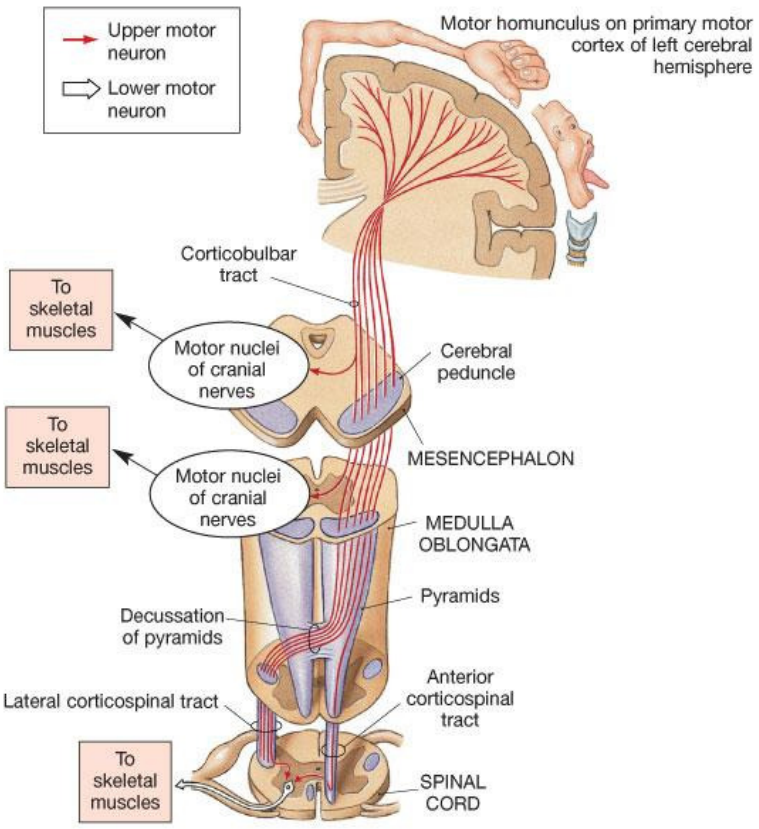

Figure 1.7 Pyramidal System [27]

1.3 Previous Methods of Filtering fNIRS

Physiological signals interfere with fNIRS measurements. These physiological signals consist of cardiac pulsation, respiration, and Mayer waves [1], [2], [11]. For typical motor cortex activation protocols the cortical hemodynamic response can be found in the 0.01 Hz to 0.4 Hz frequency range, while physiological artifacts such as cardiac pulsation can be found between 0.8 Hz to 2.0 Hz, respiration in the 0.1 Hz to 0.3 Hz range, and Mayer Waves in at about 0.1 Hz, or lower [28], [29]. Artifacts caused by respiration and Mayer waves are within the frequency range of the hemodynamic response, and cardiac pulsation is just outside of that frequency range. Thus, simple band-pass filtering cannot be used to remove these artifacts and other, more sophisticated, forms of filtering are needed [30].

A number of different filtering approaches have been explored in order to improve the fNIRS temporal signals and images [31]. Principal component analysis (PCA) is the standard method to date [30]. This method aims to remove any signal components that are common to all measurement channels and it is therefore good for removing constant background signals. More specifically, PCA decomposes baseline hemodynamic patterns into eigenvectors, and removes the eigenvectors with the largest eigenvalues from the activation data. Adaptive filtering, using a pulse oximeter as a noise reference, has also been previously implemented in a single-source, non-imaging measurement of cortical activation [32]. However, the focus of that work was to isolate the very fast neuronal responses due to finger tapping that occur at much higher frequencies than global hemodynamic signals. In [33], location-adaptive, frequency-specific algorithm was applied using an additional short fNIRS source-detector separation that only samples scalp hemodynamics, as a noise reference for filtering cardiac pulsation. In a very recent study adaptive Kalman filtering was used to predict the amplitude of global hemodynamic response in real time, as a step towards improved online monitoring of cortical activation [34] by modeling the hemodynamic response and physiological noise. The hemodynamic response was modeled as a linear combination of time-variant gamma functions, and the physiological noise

was modeled as time varying sine functions for respiration, cardiac pulsation, and Mayer waves. Of these previous methods, some did not address all three physiological artifacts mentioned, but only addressed one or two [31]-[33]. Other methods of filtering were constrained by the use of approximate model-based estimates of physiological noise and hemodynamic response [34], especially ones requiring rapid update schemes for real-time filtering of fNIRS signals [31], [34]. A method that can measure the physiological artifacts separately without any approximations, and is not restricted to real-time filtering may address some of these concerns.

1.4 Cerebral Palsy (CP)

In humans, brain damage to the primary motor cortex produces partial paralysis on the side of the body opposite the brain lesion (i.e., the contralateral side of the body). Over ten million Americans are affected by central nervous system disorders that result in motor deficits [35]. Cerebral palsy is one of these central nervous system disorders.

Cerebral palsy (CP) is caused by damage to the motor control centers of the developing brain. CP occurs in 2 per 1000 live births every year [35]. It can occur during pregnancy, childbirth, or after birth early in a child's life. CP describes the permanent disorder which prevents proper movement and posture. This disorder is often accompanied by loss of sensation, perception, cognition, communication, secondary musculoskeletal problems, and recurrent seizures [36]. One of the most prevalent types of cerebral palsy is hemiparetic CP, an incomplete paralysis of one half of the body. These motor deficits profoundly affect a child's ability to develop motor skills and to engage fully in play, exploration, and self-help activities. In order to improve their motor performance, CP patients recruit healthy portions of their brain.

Recently different brain imaging modalities have been used to assess neural plasticity in cerebral palsy children. Such modalities include electroencephalography (EEG), transcranial magnetic stimulation (TMS), and functional magnetic resonance imaging (fMRI). Many of these studies have found central motor reorganization. TMS was used along with EMG by [37], in

which they found in 64% of their hemiplegic CP patients, evidence of reorganization of the central motor pathways. A TMS study, by [38], found central motor reorganization of the arm and leg muscles in CP patients. In this study ipsilateral responses were more common among CP patients, especially in TMS of the less affected hemisphere in patients with asymmetrical brain damage. A combined TMS and fMRI study looked into the somatosensory and motor cortices in children with hemiplegic CP. This study showed a normal contralateral activation when CP subjects used their unaffected hand, but presented a bilateral or purely ipsilateral activation when CP subjects used their affected hand [39]. In another study using both TMS and fMRI, a comparison of the amount of compensatory recruitment was needed for CP subjects with small lesions and large lesions. The conclusion of the study found that the amount of corticospinal reorganization was dependent on the size of the lesion [40]. Another group, [41], used TMS and fMRI revealing a topographical reorganization of the cortical hand representations in both the intact and damaged hemispheres of CP patients. The topographical organization included the affected hemisphere and unaffected hemisphere. In [42], the authors used fMRI, and found that children with right hemiparesis of their upper extremities showed stronger ipsilateral activation than contralateral activation when moving their right fingers. They also showed that children with right hemiparesis of their upper extremities showed stronger ipsilateral activation when moving their right fingers, than in normal right handed subjects. In [43], the authors investigated the spectral and coherence EEG in children with spastic hemiplegia. Their results suggested a possible increase of plasticity in the brain for CP children.

1.5 Study Overview

The change in concentration of deoxygenated and oxygenated hemoglobin secondary to neuronal activity, known as neurovascular coupling, can be detected using functional near infrared spectroscopy (fNIRS) [11]. Similarly, fMRI detects tiny magnetization differences between HbO and Hb [44], [45]. Unfortunately, accurate imaging from fMRI often requires the

patients' complete body confinement, steadiness and minimal interference caused by motion artifacts and global hemodynamic fluctuations, for the duration of experiments, which limits the success rate to less than 50% for normal children [46]. Imaging with fNIRS is especially useful for children since it is cost effective, safe, noninvasive, and less affected by movement than other imaging modalities, such as fMRI [1].

In this work, we demonstrate that a combination of both adaptive filtering and filtering with PCA can effectively remove global hemodynamic fluctuations from fNIRS motor cortex activation signals as a post-processing step. The adaptive filtering is done using a pulse oximeter as a noise reference for cardiac pulsation, and a respiration belt as a noise reference for respiration. The subjects for this study were normal children and children with hemiparetic cerebral palsy. These subjects were recruited from an ongoing study comparing temporal and spatial differences between normal and cerebral palsy children. CP patients have difficulty controlling the movements of their limbs, thus causing more frequent motion artifacts when imaging with fMRI. In this work we only show indicative results from both pediatric groups in order to demonstrate the robustness of fNIRS methods to motion artifacts even with cerebral palsy children. Removal of global hemodynamic signals by adaptive filtering greatly improved the quality of fNIRS signals as verified by quantitative metrics. These metrics were the signal-to-noise ratio (SNR) and contrast-to-noise ratio (CNR) of detected reflectance signals at each detector, and the reconstructed image SNR. The significant improvements of these metrics conclude that concurrent measurement of global artifacts with fNIRS and the combined filtering methods may need to become standard. In fact, we show that in some instances data which seemed unusable were rescued by adaptive filtering.

In addition, we demonstrate that the improved data can potentially be used to differentiate between motor cortex activation patterns in normal children and subjects affected by hemiparetic cerebral palsy. In contrast, the pre-filtered data did not give a consistent pattern for normal children or a clear differentiation between normal children and children with cerebral

palsy. Such differences were found by using the ratio of defined duration over time-to-peak temporal metrics. Differences were also found in the areas of activation, and the distance the activation areas were from the middle of the motor cortex. Also areas were found which did not have activation according to the averaged reconstructed images, but had similar temporal responses as that of the activation area. These similar areas were found to be different in location and size between normal and CP subjects.

The following chapters describe the instrumentation setup, filtering methodology, quantitative results of signal quality after before and after filtering, and temporal and spatial differences found between normal and CP subjects. The second chapter will describe how CP subjects were assessed, the instrumentation setup, and the filtering methodology. Chapter Three presents the quantitative improvements of signal and image quality after using the described filtering. Chapter Four describes how and what temporal and spatial metrics were found to be significantly different between normal and CP subjects. Chapter Five concludes what this research has found and new directions for future studies.

CHAPTER 2

MATERIALS AND METHODS

2.1 Subjects

Five control subjects, Subjects 1 to 5 (2 female and 3 male, 8.4 +/- 2.3 years old), and five hemiparetic cerebral palsy subjects, Subjects 6 to 10 (3 female and 2 male, 8.4 +/- 2.3 years old), from the ages of 6 to 12 years, were included in this study. All the controls were right handed. Three of the cerebral palsy subjects, Subjects 6 to 8, had subcortical lesions in the left hemisphere, causing these subjects to have problems moving their right hand, and the other cerebral palsy subjects, Subjects 9 and 10 had problems moving their left hand, caused by subcortical lesions in the right hemisphere. Informed consent was obtained from all subjects, and their legal guardian/guardians. This study was approved by the Institutional Review Board at The University of Texas Southwestern Medical Center at Dallas (IRB #:042007-064). Table 2.1 is a summary of all the subjects.

Table 2.1 Summary of subjects

Subject	Gender	Age	Hemiparesis	MACS	SHUEE Score
1	Female	12	Normal	1	Spontaneous Functional Analysis – 100% Dynamic Positional Analysis – 100% Grasp/Release – 100%
2	Male	9	Normal	1	Spontaneous Functional Analysis – 100% Dynamic Positional Analysis – 100% Grasp/Release – 100%
3	Male	8	Normal	1	Spontaneous Functional Analysis – 100% Dynamic Positional Analysis – 100% Grasp/Release – 100%
4	Male	7	Normal	1	Spontaneous Functional Analysis – 100% Dynamic Positional Analysis – 100% Grasp/Release – 100%
5	Female	6	Normal	1	Spontaneous Functional Analysis – 100% Dynamic Positional Analysis – 100% Grasp/Release – 100%
6	Female	6	Right	2	Spontaneous Functional Analysis – 100% Dynamic Positional Analysis – 63% Grasp/Release – 100%
7	Female	7	Right	1	Spontaneous Functional Analysis – 100% Dynamic Positional Analysis – 100% Grasp/Release – 100%
8	Male	12	Right	1	Spontaneous Functional Analysis – 100% Dynamic Positional Analysis – 100% Grasp/Release – 100%
9	Male	8	Left	1	Spontaneous Functional Analysis – 100% Dynamic Positional Analysis – 100% Grasp/Release – 100%
10	Female	9	Left	1	Spontaneous Functional Analysis – 100% Dynamic Positional Analysis – 100% Grasp/Release – 100%

2.2 Methods of Evaluating Hemiparesis

Classification of subtypes of CP has been proposed based on the location of the lesion, part of the body affected, or the degree of impairment. Functional classification of CP children has recently been developed, two of them being the Manual Ability Classification System (MACS) [47] and the Shriners Hospital for Children Upper Extremity Evaluation (SHUEE) [48].

2.2.1 Manual Ability Classification System (MACS)

MACS was developed to classify CP children by their functional abilities in daily life [47]. MACS does not assess each hand individually, but assesses the collaboration of both hands together. The assessment focuses on handling objects in a person's individual space, as distinct from objects which are not within reach. The assessment was based on the quantity and quality of performance, also on the need of assistance, the amount of assistance, and on the adaptation needed to perform manual tasks. The classification system was made to be easily understood by both therapists and non-experts. MACS classifies a child into one of five levels, in which Level 1 being the best, and Level 5 being the worst. The description of each MACS level is given in Table 2.2.

Table 2.2 Description of each MACS level [47]

LEVEL	DESCRIPTION	DISTINCTION BETWEEN PREVIOUS LEVEL
I	**Handles objects easily and successfully.** At most, limitations in the ease of performing manual tasks requiring speed and accuracy. However, any limitations in manual abilities do not restrict independence in daily activities.	
II	**Handles most objects but with somewhat reduced quality and/or speed of achievement.** Certain activities may be avoided or be achieved with some difficulty; alternative ways of performance might be used but manual abilities do not usually restrict independence in daily activities.	Children in Level I may have limitations in handling very small, heavy or fragile objects which demand detailed fine motor control, or efficient coordination between hands. Limitations may also involve performance in new and unfamiliar situations. Children in Level II perform almost the same activities as children in Level I but the quality of performance is decreased, or the performance is slower. Functional differences between hands can limit effectiveness of performance. Children in Level II commonly try to simplify handling of objects, for example by using a surface for support instead of handling objects with both hands.
III	**Handles objects with difficulty; needs help to prepare and/or modify activities.** The performance is slow and achieved with limited success regarding quality and quantity. Activities are performed independently if they have been set up or adapted.	Children in Level II handle most objects, although slowly or with reduced quality of performance. Children in Level III commonly need help to prepare the activity and/or require adjustments to be made to the environment since their ability to reach or handle objects is limited. They cannot perform certain activities and their degree of independence is related to the supportiveness of the environmental context.
IV	**Handles a limited selection of easily managed objects in adapted situations.** Performs parts of activities with effort and with limited success. Requires continuous support and assistance and/or adapted equipment, for even partial achievement of the activity.	Children in Level III can perform selected activities if the situation is prearranged and if they get supervision and plenty of time. Children in Level IV need continuous help during the activity and can at best participate meaningfully in only parts of an activity.
V	**Does not handle objects and has severely limited ability to perform even simple actions.** Requires total assistance.	Children in Level IV perform part of an activity, however, they need help continuously. Children in Level V might at best participate with a simple movement in special situations, e.g. by pushing a simple button.

2.2.2 Shriners Hosptial of Children Upper Extremity Evaluation (SHUEE)

The SHUEE is a video-based evaluation performed by an occupational therapist, using a standardized set of objects and tasks, in order to evaluate a person's upper extremities. It was originally developed to assess upper extremity function of children with hemiplegic cerebral palsy. This evaluation process looks at the range of motion, joint stability, spasticity, spontaneous functional use of the affected extremity, and dynamic segmental positional analysis of the affected extremity [48].

There are two sections to SHUEE. The first section evaluates the subject through standard measurements of the active and passive range of motion from the shoulder to the fingers. Spasticity is evaluated using a modified version of the Ashworth scale [49]. The first section is a history-based evaluation of the performance of seven selected tasks done during daily life, and a subjective assessment of patient/family goals. The second section has three components. The first component is a spontaneous functional analysis. This evaluates the spontaneous use of the involved extremity with respect to doing nine set, common tasks. The evaluation is based off of a modified form of the House classification system [50]. The second component evaluates the segmental alignment of the effected extremity during the performance of sixteen different tasks. The final component is a grasp-and-release analysis. It evaluates the performance of the affected hand when doing grasp and release of the digits when the wrist is held in flexion, neutral, and extension.

For the second part, each component is scored separately. For each task in the spontaneous functional analysis, the first component, each task is scored from 0 (complete neglect) to 5 (independent function), giving a maximum score of 45 for this component. The dynamic positional analysis, the second component, scores each task from 0 (maximal malalignment) to 5 (optimal alignment), giving a maximum score of 60. The grasp-and-release analysis, the third component, scores each task from 0 (unable to perform) to 1 (able to

perform), giving a maximum score of 6. Each component score is represented as a percentage of the maximum score for its component.

2.3 Measurements

A 24-source, 24-detector continuous wave fNIR brain imager (CW-5) made by Techen Inc., was used to identify and map the changes of oxy-hemoglobin (HbO) and deoxy-hemoglobin (Hb) induced by motor cortex stimulation. For this work, only 16 laser sources and 16 detectors of the CW-5 system were used. Eight laser sources had a wavelength of 690 nm and the other eight had a wavelength of 830 nm. Each source location had a 690 nm and 830 nm laser source. Eight detectors were placed over each brain hemisphere so as to cover the relatively large area of the motor cortex (Figure 2.1). A 3 cm source-detector distance was set between a source and the closest of the 16 avalanche photodiode detectors. The optode placement geometry, as set on the subjects' heads by perforated Velcro straps, is shown in Figure 2.1. All cortical areas within the probes' field of view were monitored simultaneously, as the CW-5 utilizes frequency-modulation multiplexing to enable all laser sources to be on at the same time with distinct modulation frequencies from 6.4 kHz to 12.6 kHz, with an interval of 200Hz. The source modulation frequencies were much higher than the back-reflected light detection sample rate of 100.16Hz, which were later demodulated and down-sampled to 20.03Hz, to reduce data set size.

Each detector was adjacent to two sources. Each source had two lasers within a 3 cm distance of a detector, in which each detector received signals from up to four sources, two at 690 nm and two at 830 nm. The wavelengths for the laser sources in CW-5 help prevent cross-talk. Cross-talk between the HbO and Hb measurements does arise, and can be reduced by choosing optimal wavelengths. Recently, studies have shown both theoretically and experimentally that a pair of wavelengths at 660 nm to 760 nm and 830 nm provides superior separation between HbO and Hb [2], [51]. Second-nearest neighbor sources were outside of the

detectors' range (90dB). As a result there were 28 possible source-detector channel combinations, as indicated by the straight lines connecting sources to detectors in Figure 2.1.

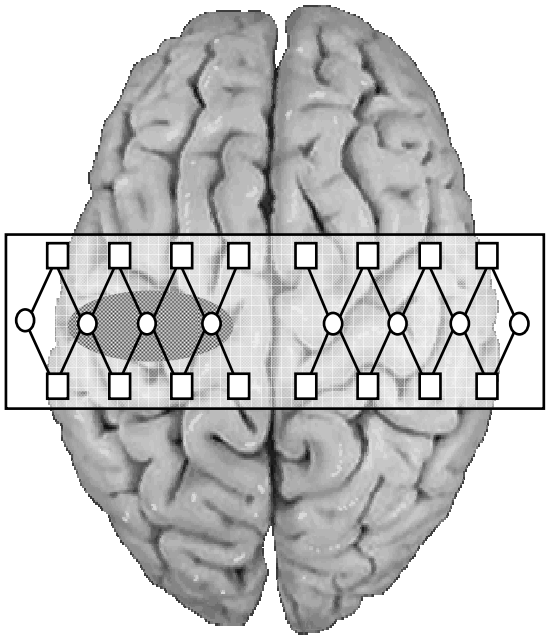

Figure 2.1 The geometry of NIRS probes on the motor cortex. The circles represent sources and the squares represent detectors.

In addition to measuring the cortical hemodynamic response by optical means, the finger tapping, respiration, and cardiac pulsation patterns were also measured simultaneously for each subject. The respiration and cardiac pulsation -- henceforth referred to as 'reference noise' -- measurements were amplified with a Brownlee Model 410 amplifier (AutoMate Scientific, Berkeley, CA), and recorded by the CW-5 system. Therefore these physiological measurements all had a common time base, which enabled their use in the adaptive filtering procedures described in Section 2.8. Finger tapping rate was measured using a custom-build, capacitance based finger tapping board which produced a bi-level continuous voltage output for each tap. Respiration patterns were measured using a respiration belt with a piezo-electric transducer (Sleepmate Technologies, Glen Burnie, MD). The belt was wrapped around each subject's chest, keeping the transducer away from the heart, in order to prevent cardiac pulsation noise from leaking into the respiration measurement. Cardiac pulsation was measured

using a pulse oximeter (Nellcor Inc., Boulder, CO) attached to the index finger on the hand not in use for tapping. In addition, muscle movement of the fingers was also measured using electromyography surface electrodes (B & L Engineering, Santa Ana, CA). These measurements were not part of our filtering procedures, but instead served as quality control sentinels for our measurements, making sure that the specified hand was the only hand tapping, while the other was kept still. A diagram of the overall instrumentation setup is shown in Figure 2.2, in which EMG (R) and EMG (L) stand for the EMG taken from the right forearm and left forearm respectfully.

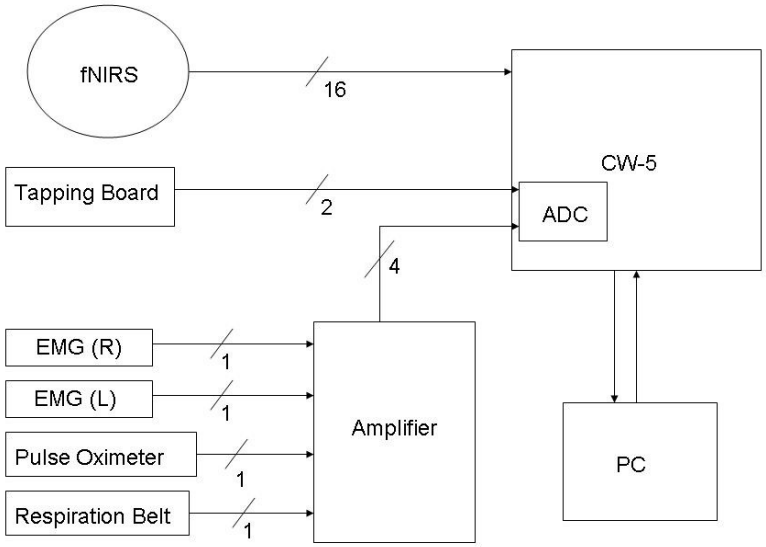

Figure 2.2 Overall Instrumentation Setup

2.4 Protocol

The CW-5, fNIRS probe placement was done according to the measured coronal (ear to ear) and sagittal (forehead to back of head) distances. The center of the probe set was placed at half the distance of the aforementioned measurements, which was considered the estimated midpoint of the motor cortex. No set tapping frequency was required of the pediatric

subjects, since the children with cerebral palsy would have difficulties following the procedure. Thus, the tapping frequency was self paced, which resulted in average finger tapping rates in the 1Hz to 2Hz range within the 15 s tapping period. Tapping consisted of moving all fingers, while the hands were held down with soft straps to keep the wrist from moving. The subjects touched the tapping board while tapping, and rested their hand on the board during the no-tapping intervals. The data acquisition protocol consisted of a 30s baseline (no tapping), immediately followed by series of ten consecutive epochs of 15s tapping and 25s of rest, and ended with a 20s baseline measurement. During the measurement the subjects watched a PowerPoint presentation in order to see when to begin and to stop tapping. Measurements were done for both left and right finger tapping. The subjects sat up straight with their head resting back in a quiet, dimly lit room. All subjects were video recorded during the measurements in order to verify that they performed the finger tapping tasks properly.

2.5 Signal and Image Processing

The time-series reflectance data acquired by the CW-5 system is usually processed by the open source software called HOMER which is implemented in Matlab and supplied by the manufacturer of CW-5. HOMER is a graphic user interface enabling users to visualize and filter reflectance signals from each detector channel, as well as, manipulate the resulting reconstructed images [52]. HOMER filters the signal using low-pass and high-pass Butterworth filters to reduce noise from frequencies outside the known physiological range. The software also applies principle component analysis (PCA) to reduce any global hemodynamic signals.

PCA can be used for retaining those characteristics of the data set which contribute most to its variance by keeping lower order principal components that often contain the "most important" aspects of the data, and ignoring higher-order ones. By decomposing the baseline data into eigenvectors, the stimulus data can be projected onto the orthogonal subspace of the noise eigenvectors, resulting in a cleaner signal as explained in [30]. In equation (2.1), **B**

represents the baseline data for all the channels. The dimension of **B** is N_t x N_c, where N_t is the number of time points and N_c is the number of channels. A spatial correlation matrix, **CM**, is then found for the baseline data.

$$\mathbf{CM} = (1/N_t) \cdot \mathbf{B} \cdot \mathbf{B}^T \quad \textbf{(2.1)}$$

The spatial correlation matrix is then decomposed into eigenvectors. Each spatial eigenvector represents a different component of the baseline signal. The eigenvectors are in matrix **E** and the eigenvalues for each eigenvector are in a diagonal matrix **D**, as shown in equation (2.2).

$$\mathbf{CM} = \mathbf{E} \cdot \mathbf{D} \cdot \mathbf{E}^T \quad \textbf{(2.2)}$$

Assuming noise is dominant in the signals, a small number, n, of spatial eigenvectors of **B** are kept. The matrix, **D**, keeps the eigenvalues in descending order. The largest eigenvalues represent the dominant noise in the signals. It is these eigenvectors that need to be removed. With the kept spatial eigenvectors representing the noise, the matrix consisting of the saved eigenvectors is represented by $\mathbf{E}_n$. If too many eigenvectors are kept, the activation signal may be lost. The rest of the signal can be projected onto an orthogonal subspace of $\mathbf{E}_n$. This will give a cleaner signal, $\mathbf{S}_{clean}$, as shown in equation (2.3) [30].

$$\mathbf{S}_{clean} = (\mathbf{I} - \mathbf{E}_n \cdot \mathbf{E}_n^T) \quad \textbf{(2.3)}$$

The HOMER software also de-trends the signal to reduce any long term drifts and averages the detected signal for individual source-detector pairs over user-selected task intervals of tapping and rest. Subsequently, activation images are reconstructed by use of the Tikhonov perturbation solution to the photon diffusion equation [53] that employs a regularized

Moore-Penrose inversion scheme [54]. The reconstructed two-dimensional images represent maps of Hb and HbO changes on the brain cortex surface, within the detector's field of view (rectangle in Figure. 2.1) as a result of finger tapping.

2.6 Baseline Correction

In HOMER, the baseline is defined as the first data point received or an average over a selected number of data points at the very beginning of data acquisition. However baseline drift could occur throughout the repeated cycles of activation and rest in these experiments. HOMER does not currently let the user re-define a baseline for individual activation intervals. Code in Matlab was written to correct for the baseline before each activation interval by taking the average of the five seconds of data before the beginning of each activation interval and then subtracting that value from the activation data in that interval. After each activation interval was baseline corrected, selected intervals were averaged together. Corrected baseline values resulted in better signal contrast from the background in reconstructed images and therefore improved image contrast.

2.7 Delay Correction

Since the noise reference measurements were not taken at the same anatomical locations as the fNIRS measurements, there were time delays between the cardiac and respiratory noise reference signals and fNIRS signals. Cross-correlation calculations were performed to estimate the delay between reference noise measurements and fNIRS signals. If the cross-correlation peak value was ahead of the midpoint there was a delay between the measured noise and the noise in the fNIRS [55]. The cross-correlation was found by equation (2.4), where cc(k) is the cross-correlation at sample point l, L is the length of v(k), v(k) is the fNIRS signal, and n(k) is the noise reference signal.

$$cc(x) = \sum_{k=0}^{L} v(k)\, n(l-k) \qquad \textbf{(2.4)}$$

The fNIRS signal was band-pass filtered between 0.8Hz and 2.0Hz, the known range of cardiac pulsation frequencies at rest [2], and cross-correlated with the cardiac pulsation noise reference to estimate the time delay between the two signals. The fNIRS signal was also band-pass filtered between 0.25Hz and 0.6Hz, the known range of respiration frequencies at rest [2], and cross-correlated to check if there was a delay with respect to the respiration noise reference. Sample cross-correlations for cardiac pulsation and respiration are shown in Figure 2.3 No significant delays were found for cardiac pulsation, but delays were found from 0s to 3s for respiration. Figure 2.3(b) demonstrates this point as the solid vertical line indicates that the cross-correlation peak is shifted from the zero delay time.

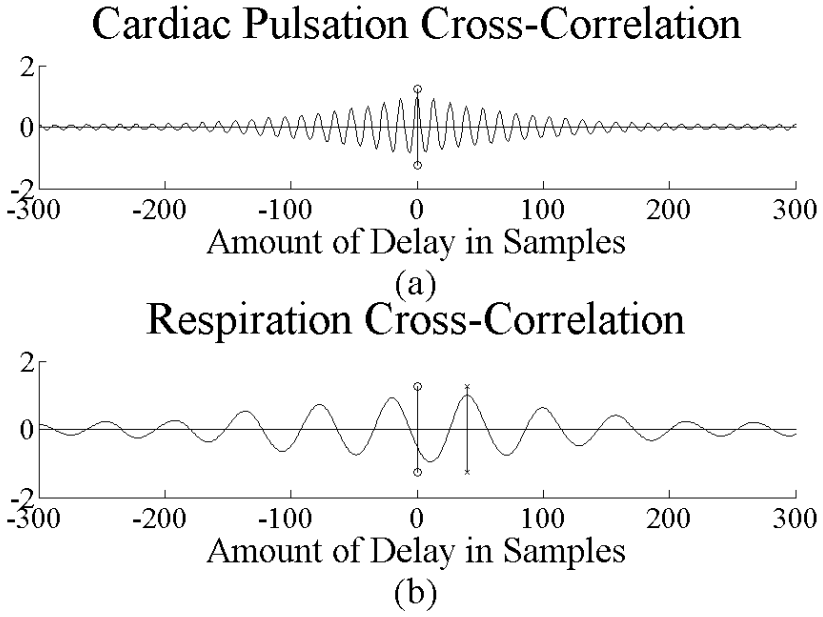

Figure 2.3 (a) Cross-correlation of the pulse oximeter signal to the fNIRS cardiac pulsation frequency range signal. (b) Cross-correlation of the respiration belt signal to the fNIRS respiration frequency range signal. Since the sampling frequency was at 20Hz, each sample represents 0.05s.

Once the respiration signal delay was computed for each subject the reference noise signal was time-shifted, by appropriate zero buffering, so it would be in synchrony with the fNIRS signal for that subject. The length of buffering was equal to the number of samples of delay. The buffer was added at the end of the noise reference signal. Subsequently adaptive filtering was employed to remove the reference noise from the fNIRS signal as follows.

2.8 Adaptive Filtering

One of the main advantages of adaptive filtering is its capability to follow changes in a signal. Since biomedical signals are generally non-stationary, adaptive filtering has the potential of being a good fit for fNIRS applications [32].

The flowchart of our signal processing methodology is shown in Figure 2.4. In this figure, the evoked brain hemodynamic changes in HbO and Hb are the target measurements denoted by a vector **v(t)** with elements of v_i. The subscript *i* is the index of the sample point for each signal sample (20Hz sampling frequency). The concurrent physiological measurements are respiration, **r(t)**, and cardiac pulsation, **c(t)**. To exclude frequencies which are outside the known range of the signals of interest, the fNIRS signal was first band-pass filtered between 0.01Hz and 2Hz, using an eighth order Butterworth filter. Also, to reduce electronic noise from the cardiac and respiration reference signals, they were low-pass filtered at 5Hz (not shown in Figure 2.4). Additionally, baseline correction and then PCA were employed, as described above. We empirically found that removing the two largest eigenvalues resulted in the best compromise between reducing global background signal while not substantially reducing the contrast of activation areas in the reconstructed images. After PCA, using a Least Mean Squares adaptive filter [56], [57], the signal was filtered for respiration first, and then cardiac pulsation, as shown in Figure 2.4. The adaptive filters were designed separately for cardiac pulsation and respiration artifacts. The general equations for the adaptive filter are given in equations (2.5) and (2.6). *M* represents the order of the filter and the w_k values are the filter

coefficients, where k is the coefficient index. Since the coefficients were adjusted by the filter output e_i on a sample by sample basis, we use $w_{k,i}$ to denote the kth coefficient at time i. Coefficients were updated by a least mean square (LMS) algorithm that is simple and fast [56], [57]. The LMS algorithm for optimization is

$$e_i = v_i - \sum_{k=1}^{M} w_{k,i} x_{i-k} \quad \textbf{(2.5)}$$

$$w_{k,i} = w_{k,i-1} + 2u e_i x_{i-k} \quad \textbf{(2.6)}$$

where the constant u is a step size, which controls the convergence rate of the algorithm, and x_i is the reference noise signal [56]. The initial 30s of baseline were used to initialize the weights when filtering both respiration and cardiac pulsation. Two parameters, the update step and the number of coefficients, needed to be chosen for each filter. Ideally a large update step and a large number of coefficients are wanted for adaptive filtering. A large update step is desired for faster convergence, and a large number of coefficients are desired to minimize error of the adaptive filter. Since these two parameters are inversely proportional to the filter convergence speed in equation (2.5), a trade-off was taken [56].

The update step was bounded, as seen in equation (2.7), in order to maintain stability of the adaptive filter. In equation (2.7), M is the number of coefficients, u is the update step, and P_{vv} is the power of the signal. Values of M and u were found empirically.

$$0 < u < 1/[MP_{vv}] \quad \textbf{(2.7)}$$

The adaptive filter for respiration had 600 coefficients. The coefficients defined a time window of length directly proportional to the signal sampling frequency. In our measurements the signal was sampled at approximately 100 Hz and then down-sampled to about 20Hz. Therefore a

window length of 600 coefficients was needed to cover 30s, which spanned about ten respiratory cycles. Following similar considerations the adaptive filter for cardiac pulsation had 100 coefficients to capture several heart beat periods for a length of 5s. Then the sampled reference signals were sequentially filtered out of the fNIRS signal from each detector, as outlined in Figure 2.4, using a LMS algorithm [56], [57]. It was empirically found that filter convergence was always attained with fractional update steps of $1x10^{-4}$ and $3x10^{-4}$ for the respiration and cardiac reference noise coefficients, respectively.

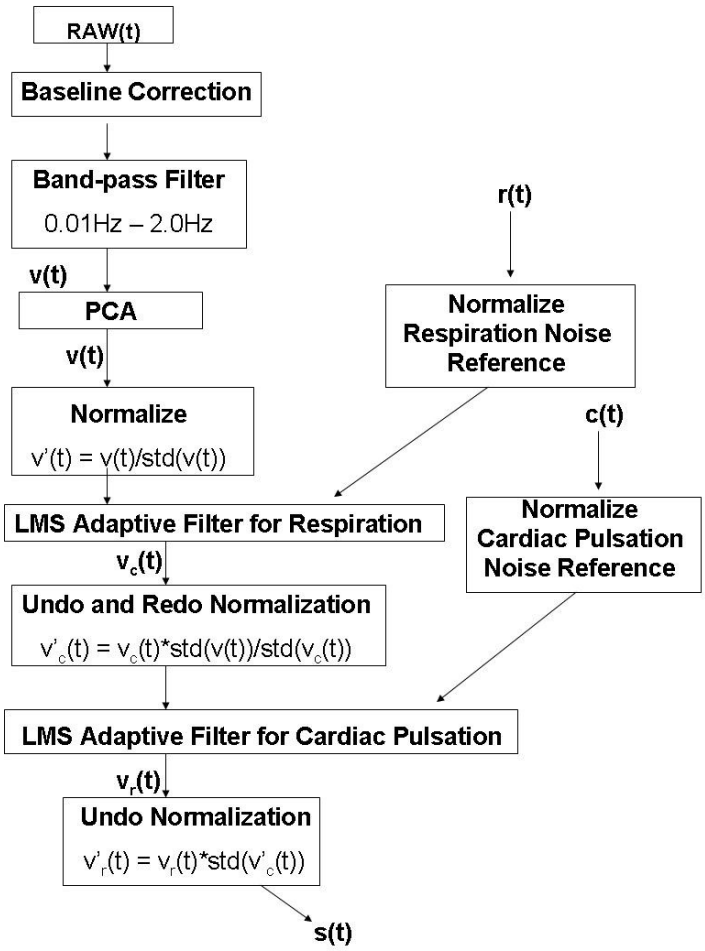

Figure 2.4 Flowchart of the Signal Processing Algorithm

2.9 Averaging

In order to further reduce the noise in the signal, we only included in our data analysis the tapping-rest intervals for which we could confirm that finger tapping was executed properly without any extra body movements, as judged from the video recording of the experiments. The resulting filtered and averaged data in all detector channels were fed into the HOMER software so that activation images could be reconstructed [52]. Images were reconstructed from 5s to 20s of activation, which was the time window during which most of the activation signal was observed.

Though measurements at 690 nm and 830 nm enable simultaneous determination of HbO and Hb dynamics, in this work we have focused on the analysis of HbO signals. We have found that Hb signals were weaker, due to the aforementioned blood flow overcompensation in activated areas, but nevertheless yielded qualitatively similar results in our analyses.

CHAPTER 3

RESULTS OF FILTERING

We have employed temporal and spatial metrics to quantify any improvements in the quality of detected time-series signals at each detector as well as the quality of the reconstructed images, before and after application of our filtering algorithm.

3.1 Temporal Signal-to-Noise Ratio

The SNR was measured for our time-series reflectance measurements at each detector channel. The fNIRS based activation SNR was computed as the ratio of the measured reflectance signal power, i.e. the area under the spectrum, during activation to the power of the measured baseline signal. The signal was considered as baseline when the subject was at rest (first 30s and last 20s of data acquisition plus the last 10s of every tapping-rest cycle). In this analysis we considered signals in the 0.01Hz to 2.0Hz range. Signal powers were computed by use of the Welch method [57]. The power spectra were estimated using 25% overlapping hamming windows of 400 samples, which is equivalent to a window length of 20s.

The SNR was subsequently calculated for each detector channel, by equation (3.1) where P_s is the area of the power spectrum for the signal, and P_n is the area of the power spectrum for the baseline between 0.01Hz and 2.0Hz.

$$SNR = 10*\log(P_s/P_n) \quad \textbf{(3.1)}$$

The change of the SNR for each channel with activation for Subject 1 is presented in Figure 3.1. The number of channels with activation varied from subject to subject. From Figure 3.1, it can

be seen that the active channel SNRs are larger after filtering. Similar results were also seen in the subjects with cerebral palsy, as shown in Figure 3.2. In order to check the improvement of SNR from before filtering to after filtering, a one sampled t-Test was performed using SAS 9.1. The null hypothesis was defined as no average improvement in SNR after filtering the fNIRS signals for channels with activation. A statistical significance level of P = 0.05, or a 95% confidence interval, was used. The results of the t-Test, shown in Table 3.1, concluded that there was a significant improvement in the SNR after filtering with $p < 0.0001$.

Table 3.1 One sampled paired t-Test for SNR

	Mean	Standard Deviation
Not Filtered	9.99 dB	6.68 dB
Filtered	13.62 dB	5.65 dB

T-Test			
N	DF	t Value	Pr > |t|
88	87	1.66	< 0.0001

Power (1-β) = 0.99

The improvement of SNR from before to after filtering was also checked for the normal subject group and CP subject group separately. One sampled t-Tests were performed using SAS 9.1. The null hypothesis was defined as no average improvement in SNR for each group after filtering the fNIRS signals for channels with activation. A statistical significance level of P = 0.05, or a 95% confidence interval, was used. The results of the t-Tests, shown in Tables 3.2 and 3.3, concluded that there was a significant improvement in the SNR after filtering with $p = 0.0387$ for normal subjects and $p < 0.0001$ for CP subjects. Seven additional normal subjects are needed in order to increase the statistical power to 0.90.

Table 3.2 One sampled paired t-Test for SNR of only normal subjects

	Mean	Standard Deviation
Not Filtered	13.35 dB	7.07 dB
Filtered	15.16 dB	7.26 dB

T-Test			
N	DF	t Value	Pr > |t|
30	29	1.70	0.0387

Power (1-β) = 0.557

Table 3.3 One sampled paired t-Test for SNR of only CP subjects

	Mean	Standard Deviation
Not Filtered	7.43 dB	5.18 dB
Filtered	11.90 dB	5.58 dB

T-Test			
N	DF	t Value	Pr > |t|
58	57	1.67	<0.0001

Power (1-β) = 0.99

Figure 3.3 demonstrates the effect of filtering the time-resolved fNIRS signal of an activation channel averaged over 10 tapping-rest cycles, for Subject 1. Our power spectrum analysis indicated that the big dips on either side of the signal peak in the pre-filtered curve in Figure 3.3 were mainly due to baseline signals in the 0.01Hz to 0.4Hz range, which corresponded to Mayer waves and respiration. The smaller variation in the signal, riding on the hemodynamic response, is cardiac pulsation, which was found to be in the range of 0.8Hz to 1.5Hz.

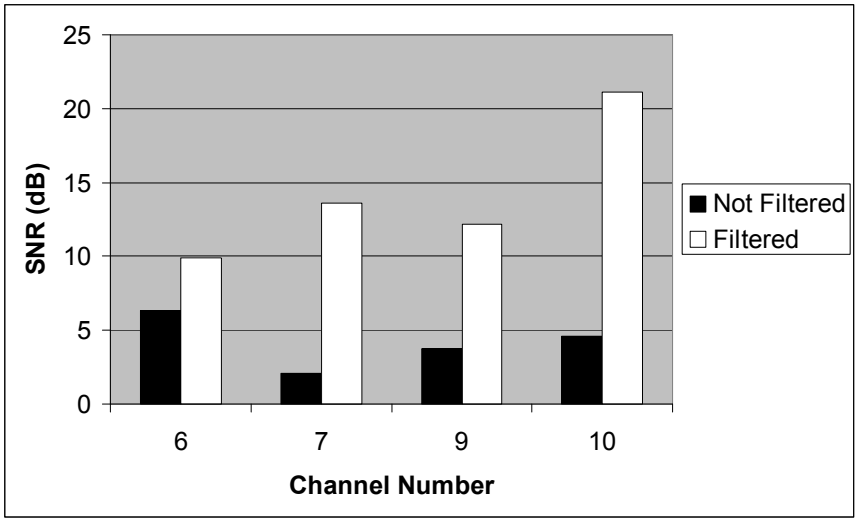

Figure 3.1 The SNR of active channels, before and after filtering, results are for Subject 1 (normal subject) tapping with right finger. Channels 1 to 14 were located on the left hemisphere, and channels 15 to 28 on the right hemisphere of the motor cortex. For Subject 1 channels 6, 7, 9, and 10 were the only ones with activation.

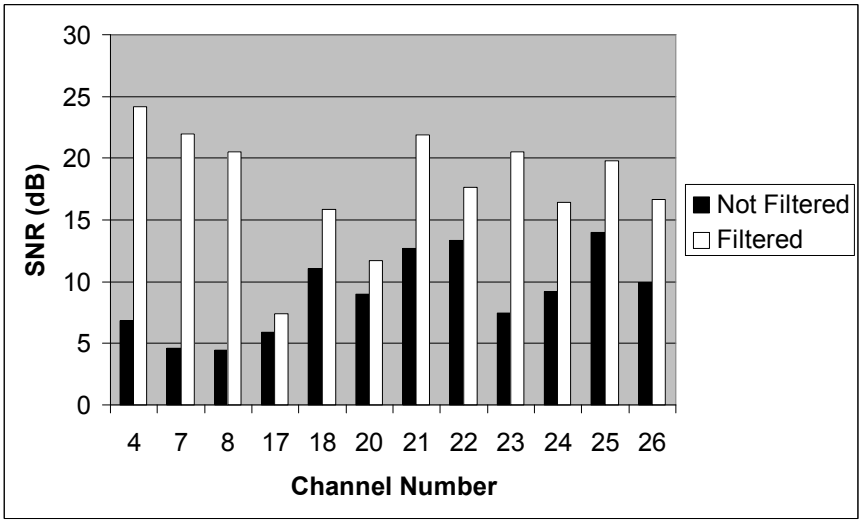

Figure 3.2 The SNR of active channels, before and after filtering, results are for Subject 10 (cerebral palsy subject) tapping with left finger. Channel placement as in Figure 3.1, above. For Subject 10 the channels shown in this graph were the only ones with activation.

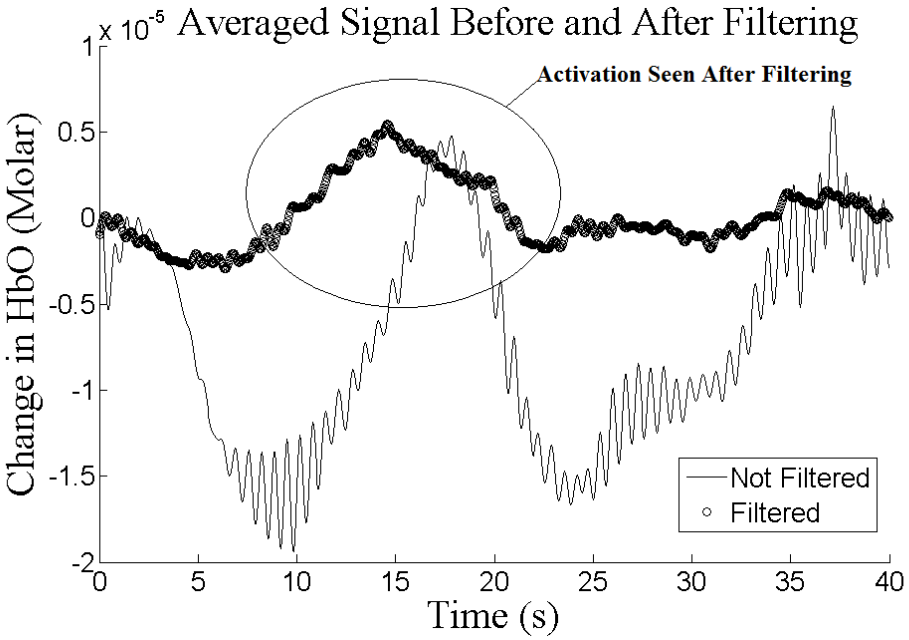

Figure 3.3 Temporal signal averaged over 10 tapping-rest cycles before (thin curve) and after (thick curve) filtering. The encircled area indicates where activation is seen after filtering.

The amount of improvement in the SNR for each experiment was variable and depended on the intensity of detected activation signals versus baseline signals for each subject. A large fraction of the baseline signals originates from the scalp hemodynamics [2]. Variations in the latter as well as variations in the quality of detector-scalp optical contact and differences in tissue optical properties and geometry between subjects are all potential contributors to these variations. Nevertheless it is worthwhile observing Figures 3.1 to 3.3 and the one sample paired t-Test results that are representative of the significant SNR improvements seen in all subjects.

3.2 Contrast-to-Noise Ratio

We have empirically determined that looking at only SNR can sometimes be deceiving, since in some cases deactivation can cause large SNR values before filtering. To remedy this potential shortcoming, CNR can be used as a complementary metric to quantify activation signal change. CNR values depend on the mean and standard deviation of the baseline and

activation hemodynamic responses, whereas SNR only depends on the signal power during the activation interval. Thus, CNR may serve as a quantitative and intuitive parameter to assess how well global hemodynamics detected during the rest periods affect the amplitude of detected neuronal activation during tapping periods. The average CNR over the course of each experiment was first computed for each detector using the following equation

$$\mathrm{CNR} = [\mathrm{mean}(\mathbf{dur}) - \mathrm{mean}(\mathbf{pre})]/[\mathrm{std}(\mathbf{dur})^2 + \mathrm{std}(\mathbf{pre})^2]^{1/2} \quad \textbf{(3.2)}$$

where **pre** represents the 10s prior to the beginning of tapping (-10s to 0s) and **dur** represents 10s of tapping (5s to 15s) a point at which the activation is at its highest in each activation cycle [30]. To compare results between signals before and after filtering, the average CNR of the channels without activation were first subtracted from the average CNR of the channels with activation. The resulting ratios of net CNR values before and after filtering were expressed as a percentage change in Figure 3.4. The average net CNR change over all subjects was 96%. However large variations between subjects were seen. In some cases, the gain in CNR was many fold, while in other subjects, such as Subject 4, there was little CNR gain, because its value was large to begin with.

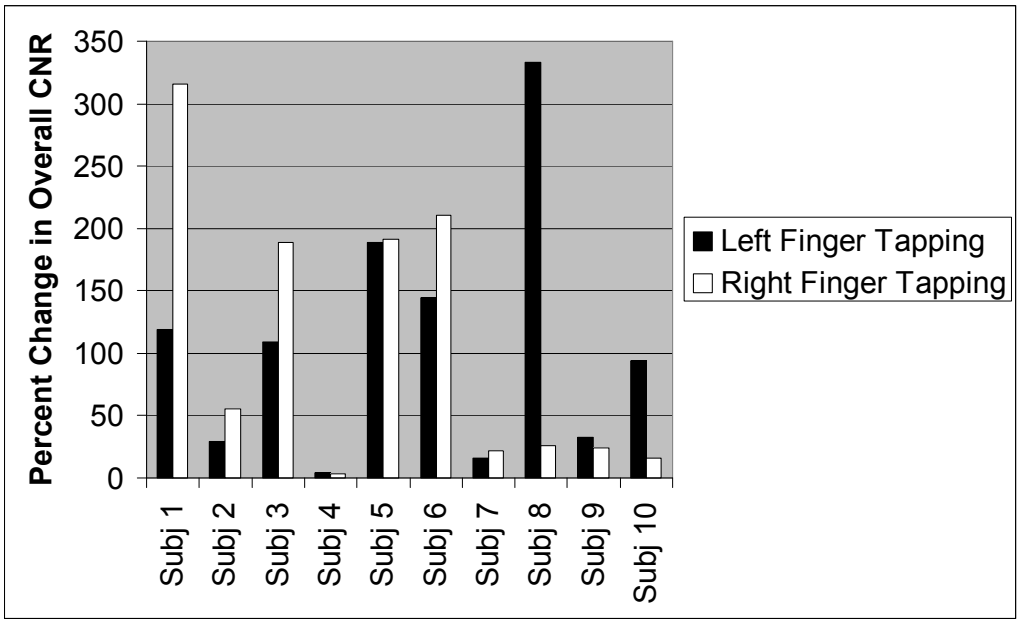

Figure 3.4 Percent change in time-averaged net CNR over the length of each experiment. Subjects 1 to 5 were normal subjects and Subjects 6 to 10 were subjects with cerebral palsy.

In order to check the improvement of net CNR from before filtering to after filtering, a one sampled t-Test was performed using SAS 9.1. The null hypothesis was defined as no average improvement in the net CNR after filtering the fNIRS signals. A statistical significance level of P = 0.05, or a 95% confidence interval, was used. The results of the t-Test, shown in Table 3.4, concluded that there was a significant improvement in the net CNR after filtering with $p < 0.0001$.

Table 3.4 One sampled paired t-Test for net CNR

	Mean	Standard Deviation
Not Filtered	1.87	1.39
Filtered	3.18	1.75

T-Test			
N	DF	t Value	Pr > |t|
24	23	1.72	< 0.0001

Power (1-β) = 0.99

The improvement in net CNR from before filtering to after filtering was also checked for the normal subject group and CP subject group separately. One sampled t-Tests were performed using SAS 9.1. The null hypothesis was defined as no average improvement in net CNR for each group after filtering the fNIRS signals. A statistical significance level of P = 0.05, or a 95% confidence interval, was used. The results of the t-Tests, shown in Tables 3.5 and 3.6, concluded that there was a significant improvement in the net CNR after filtering with p = 0.0005 for normal subjects and p = 0.0006 for CP subjects.

Table 3.5 One sampled paired t-Test for net CNR of only normal subjects

	Mean	Standard Deviation
Not Filtered	2.30	1.89
Filtered	3.80	2.12

T-Test			
N	DF	t Value	Pr > |t|
10	9	1.83	0.0005

Power (1-β) = 0.997

Table 3.6 One sampled paired t-Test for net CNR of only CP subjects

	Mean	Standard Deviation
Not Filtered	1.51	0.67
Filtered	2.27	0.96

T-Test			
N	DF	t Value	Pr > |t|
14	13	1.83	0.0006

Power (1-β) = 0.989

3.3 Signal-to-Noise Ratio for Reconstructed Images

Time series images of HbO change over the detectors' field of view, located over the subjects' motor cortex (Figure 2.1), were reconstructed for every 0.05 s interval of the fNIRS measurements. Measurements at each time interval were averaged over 10 activation rest cycles prior to image reconstruction. Image SNR was computed on the average image of the time-series images within the 5s to 20s time points, which represented the time interval where

most of the activation occurred in a tapping-rest cycle (e.g. Figure 3.3). A clustering algorithm in Matlab was written, based on the k-means algorithm [58], to separate activation from baseline areas. The algorithm employed three clusters that were initialized at the maximum, zero, and minimum pixel values. The algorithm then placed each image pixel into one of the clusters. If the pixel value distance was closest to a specific cluster mean, then that pixel was placed into that cluster. The distance was defined by the Euclidean distance in equation (3.3), where Distance is the distance being calculated between a pixel value located at an x and y coordinate on the image and the mean of each of the three clusters [59].

$$Distance_{cluster}(x,y) = |pixel\_value(x,y) - mean_{cluster}| \quad \textbf{(3.3)}$$

The algorithm recalculated the mean of each cluster after processing the whole image and repeated the process until the means of each cluster no longer changed, in which a maximum of 11 iterations were necessary. The cluster which initially had a mean equal to the maximum value in the image represented pixel values related to activation. The cluster which initially had a mean equal to zero represented pixel values related to noise. Similarly, the cluster which initially had a mean equal to the minimum value in the image represented deactivation. The SNR of the image was measured by taking the average of the cluster which represented activation and dividing it by the average value of the cluster which represents noise. Figure 3.5 shows that for most subjects the activation image SNR is significantly higher after filtering. On the other hand Subjects 2 and 4 show a slight decrease in their image SNR in Figure 3.5. The origin of this effect is that filtering is imperfect and inevitably removes some of the signal along with the noise, which was noticeable in these high SNR cases. However, the decrease in SNR for these subjects were not large, whereas in the cases where filtering increased SNR the improvements were very large.

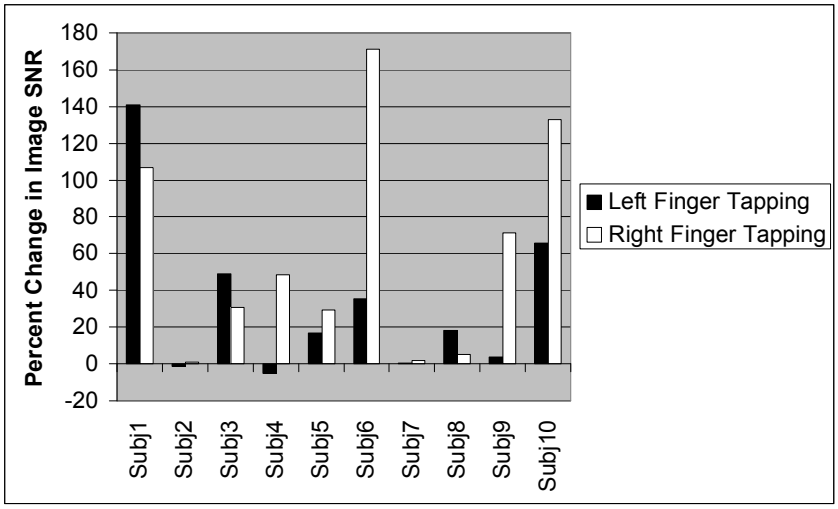

Figure 3.5 Percent change of the time-averaged activation image SNR after filtering. Subjects 1 to 5 were normal, and Subjects 6 to 10 were subjects with cerebral palsy.

It is important to note in some cases the improvement of the images due to filtering allowed the analysis of data to be carried out. Otherwise, the collected data would not have been of use. An example is shown in Figure 3.6 where, prior to filtering, Subject 1 demonstrated deactivation in both hemispheres despite tapping with the right hand. After filtering, an activation area could be seen in the left hemisphere, as was expected. Our filtering procedure produced such significant improvements in two cases involving normal subjects.

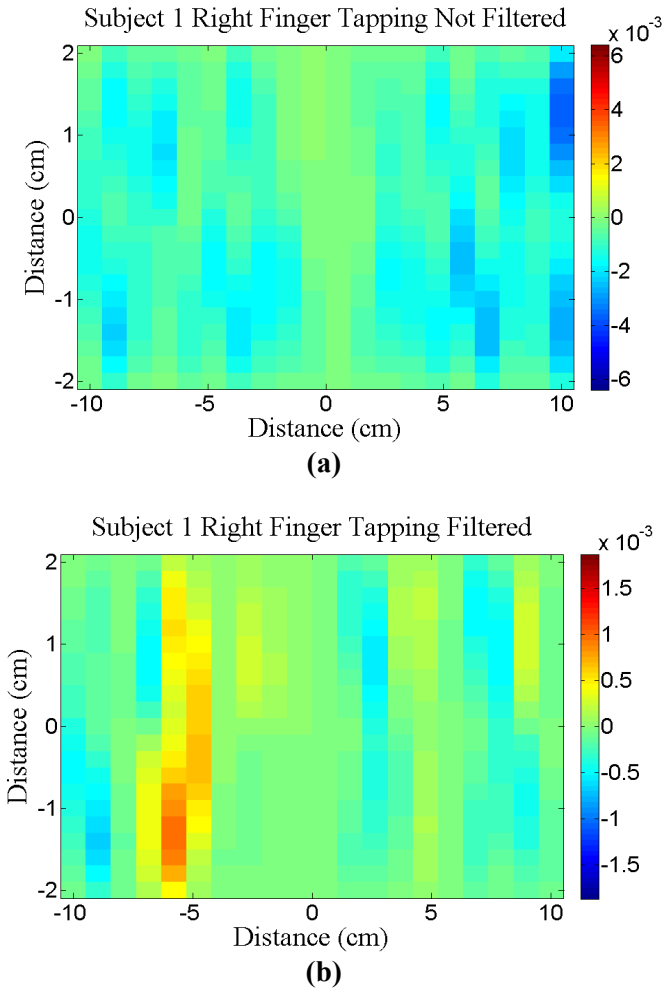

Figure 3.6 Averaged HbO images for Subject 1 (a) before and (b) after filtering. Notice the deactivation represented in both hemispheres when the signals are not filtered. After filtering, an activation area is seen in the left hemisphere.

In order to compare the image SNR from before filtering to after filtering, statistical analysis was performed using SAS 9.1. The null hypothesis was defined as no average improvement in SNR after filtering the fNIRS signals for channels with activation. After finding that the image SNR data was significantly not normally distributed, by the Shapiro-Wilk test, a one sampled Wilcoxon Signed-Rank test was performed to see if there was a significant improvement in the image SNR after filtering. A statistical significance level of P = 0.05, or a 95% confidence interval, was used. The results of the non-parametric test, shown in Table 3.7,

concluded that there was a significant improvement in the image SNR after filtering with a p-value of 0.0014.

Table 3.7 Wilcoxon Signed-Rank test for image SNR

	Mean	Standard Deviation
Not Filtered	1.87	1.39
Filtered	3.18	1.75

Wilcoxon Signed-Rank Test

N	DF	S Value	Pr > |t|
24	23	60	0.0014

The improvement in image SNR from before filtering to after filtering was also checked for the normal subject group and CP subject group separately. A one sampled t-Test was performed for the normal subjects, and the Wilcoxon Signed-Rank test was performed for the CP subjects since their data was not normally distributed according to the Shapiro-Wilk test, using SAS 9.1. The null hypothesis was defined as no average improvement in image SNR for each group after filtering the fNIRS signals. A statistical significance level of P = 0.05, or a 95% confidence interval, was used. The results of the Wilcoxon Signed-Rank tests, shown in Tables 3.8 and 3.9, concluded that there was a significant improvement in the image SNR after filtering with p = 0.0048 for normal subjects and p = 0.0257 for CP subjects.

Table 3.8 One Sampled t-Test for image SNR of only normal subjects

	Mean	Standard Deviation
Not Filtered	1.61	0.40
Filtered	2.12	0.21

T-Test

N	DF	t Value	Pr > |t|
10	9	1.83	0.0048

Power (1-β) = 0.915

Table 3.9 Wilcoxon Signed-Rank test for image SNR of only CP subjects

	Mean	Standard Deviation
Not Filtered	2.02	0.59
Filtered	2.71	1.48

Wilcoxon Signed-Rank Test

N	DF	S Value	Pr > |t|
14	13	31	0.0257

CHAPTER 4

DIFFERENCES BETWEEN NORMAL AND CEREBRAL PALSY SUBJECTS

4.1 Time-to-Peak and Duration of the Temporal Signals

After having filtered the detected signals, we empirically selected time-to-peak and duration of activation per tapping cycle as temporal metrics to assess differences between normal and cerebral palsy children. The time-to-peak was found by detecting local maxima in the averaged time series signals. This information was then sorted and their maximum value was found. Using the peak temporal location, the time-to-peak was computed from the beginning of the activation interval.

In order to compute activation duration, the averaged temporal signals were concatenated together to form a two-dimensional spatial-temporal plot. The clustering algorithm used to find the image SNR was then used to separate the activation areas from background noise. Anything above the maximum value of the noise cluster was considered activation. For the channels with activation, the amount of time that activation lasted above the maximum noise value was considered as the duration for that channel. In Figure 4.1, both time-to-peak and duration, represent averaged values for the processed data from all channels where activation was detected, are shown.

A consistent pattern was seen among the normal subjects when a ratio of duration over time-to-peak was calculated after filtering the fNIRS signals. Filtering was needed to help differentiate between normal and cerebral palsy children. Consistent results were not seen across normal subjects before filtering. For example, Subject 1 had a much larger time-to-peak than duration when left finger tapping as could be seen from the effects of filtering from Figure 3.3. After filtering, all normal subjects had a ratio of one or greater for both right and left finger

tapping (Figure 4.1). Hence, for normal subjects, the duration was greater than or equal to the time-to-peak. In Figure 4.1 normal subjects have a black filled bar for left finger tapping and white bar for right finger tapping. This finding was not the same for cerebral palsy children (Figure 4.1). For all cerebral palsy subjects the duration was found to be less than the time-to-peak when the subject was tapping with their affected hand. In the case of four of the cerebral palsy subjects, Subjects 6 to 9, the duration was at least two times larger than the time-to-peak when the subjects were tapping with their non-affected hand. Although cerebral palsy subjects may on occasion give normal metrics for their non-affected hand, the affected hand will give abnormal metrics, or both hands will give abnormal metrics as seen in Figure 4.1. Therefore it appears necessary that both left and right hand tapping be performed as part of the protocol to differentiate between healthy children and children with cerebral palsy. In Figure 4.1 cerebral palsy children with right hemiparesis, Subjects 6 to 8, have a horizontal brick pattern for left finger tapping and a dotted pattern for right finger tapping, and left hemiparesis subjects, Subjects 9 and 10, have a tressel pattern for left finger tapping and a horizontal line pattern for right finger tapping.

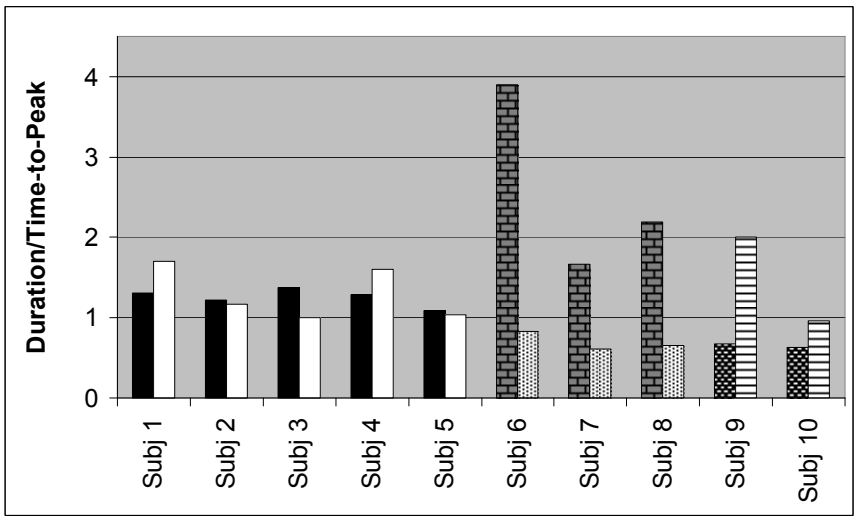

Figure 4.1 Bar graph presenting the ratio of duration over time-to-peak metrics for both right finger (right vertical bar) and left finger tapping (left vertical bar). Subjects 1 to 5 were normal subjects, Subjects 6 to 8 were right hemiparesis cerebral palsy subjects, and Subject 9 and 10 were left hemiparesis cerebral palsy subjects.

Firstly, a difference in ratio of duration over time-to-peak between normal subjects left finger tapping and right finger tapping was checked. Using SAS 9.1, a two sampled t-Test was performed to see if there was a significant difference between the means of the ratios for normal subjects left finger tapping and right finger tapping. The null hypothesis was defined as no mean difference in the duration over time-to-peak ratio. A statistical significance level of P = 0.05, or a 95% confidence interval, was used. The results of the two sampled t-Test, shown in Table 4.1, concluded that there was no significant difference between the means of the duration over time-to-peak ratio between normal subjects left finger tapping (LFT) and right finger tapping (RFT). The p-value was shown to be equal to 0.79.

Table 4.1 Two sampled t-Test of the ratio of duration to time-to-peak between normal subjects left finger tapping and right finger tapping

	N	Mean	Standard Deviation
LFT	5	1.26	0.11
RFT	5	1.29	0.32

Two Sample t-Test

DF	t-Value	Pr > |t|
8	-0.27	0.7900

Power (1-β) = 0.057

From Figure 4.1, when CP subjects were tapping with their affected hand, their duration over time-to-peak ratio was consistently less than one. A two sampled t-Test was performed, using SAS 9.1, to see if there was a significant difference between the means of the ratios for normal subjects and for CP subjects tapping with their affected hand. Since there was no significant difference between the ratio of normal subjects tapping with their right or left hand, the ratios of the right and left finger tapping were put into one group for the normal subjects. The null hypothesis was defined as no mean difference in the duration over time-to-peak ratio

between normal subjects and CP subjects tapping with their affected hand. A statistical significance level of P = 0.05, or a 95% confidence interval, was used. The results of the two sampled t-Test, shown in Table 4.2, concluded that there was a significant difference between the means of the duration over time-to-peak ratio between normal subjects and CP subjects tapping with their affected hand. The p-value was shown to be less than 0.0001.

Table 4.2 Two sampled t-Test of the ratio of duration to time-to-peak between normal subjects and CP subjects

	N	Mean	Standard Deviation
Normal	10	1.28	0.23
CP	5	0.68	0.09

Two Sample t-Test

DF	t-Value	Pr > |t|
13	5.55	< 0.0001

Power (1-β) = 0.99

4.2 Time-to-Peak and Duration of the Reconstructed Images

Images were reconstructed for every 0.05 s, thus giving temporal information for every pixel in the image. The same metrics of time-to-peak and duration were found for each pixel. The time-to-peak algorithm was the same, since each pixel is looked at individually, as were the detector signals. Previously, for the duration algorithm for the detector signals, the signals were concatenated to give a two-dimensional spatio-temporal image. The clustering algorithm was then able to define activation areas based from the image. In order to do a similar duration measurement, the Euclidean distance is redefined to handle each pixel value in a three-dimensional space, since we are looking at images over time. The Euclidean distance is redefined in equation (4.1), where Distance is the calculated Euclidean distance, pixel_value is

the value of the pixel on the x and y coordinate of the image at a certain time point, and $mean_{cluster}$ is the mean of the specified cluster [59].

$$Distance_{cluster}(x,y,t) = |pixel\_value(x,y,t) - mean_{cluster}| \quad \textbf{(4.1)}$$

The pixels were divided into three clusters; one for activation, one for noise, and one for deactivation. The algorithm recalculated the mean of each cluster after processing the whole image and repeated the process until the means of each cluster no longer changed, in which a maximum of 20 iterations were necessary. The cluster which initially had a mean equal to the maximum value in the image represented pixel values related to activation. The cluster which initially had a mean equal to zero represented pixel values related to noise. Similarly, the cluster which initially had a mean equal to the minimum value in the image represented deactivation. Figure 4.2, which is labeled the same as Figure 4.1, gives similar results as those shown in Figure 4.1.

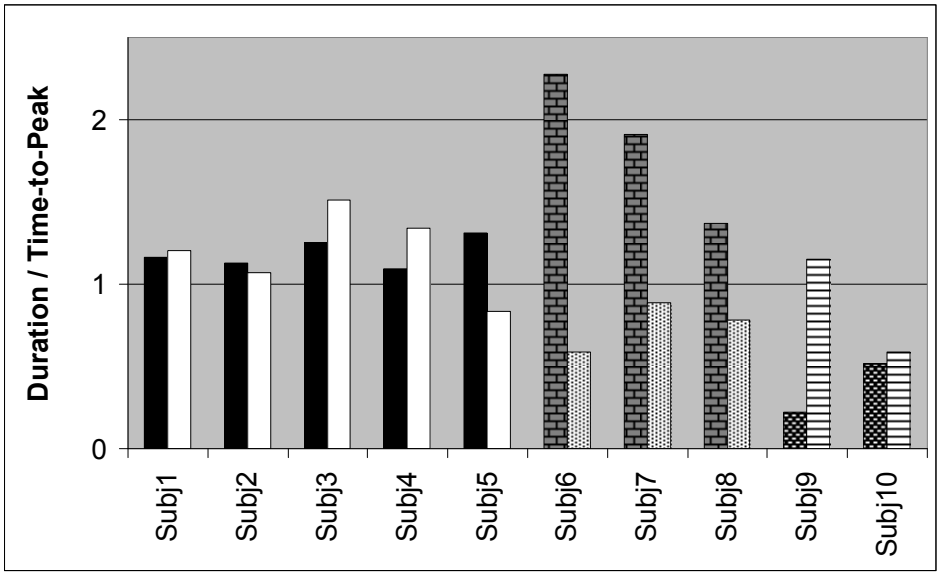

Figure 4.2 Bar graph presenting the ratio of duration over time-to-peak metrics for both right finger (right vertical column) and left finger tapping (left vertical column) for the reconstructed images. Subjects 1 to 5 were normal subjects, Subjects 6 to 8 were right hemiparesis cerebral palsy subjects, and Subject 9 and 10 were left hemiparesis cerebral palsy subjects.

First a difference in ratio of duration over time-to-peak between normal subjects left finger tapping and right finger was checked. Using SAS 9.1, a two sampled t-Test was performed to see if there was a significant difference between the means of the ratios for normal subjects left finger tapping and right finger tapping. The null hypothesis was defined as no mean difference in the duration over time-to-peak ratio. A statistical significance level of P = 0.05, or a 95% confidence interval, was used. The results of the two sampled t-Test, shown in Table 4.3, concluded that there was no significant difference between the means of the duration over time-to-peak ratio between normal subjects left finger tapping (LFT) and right finger tapping (RFT). The p-value was shown to be equal to 0.9874.

Table 4.3 Two sampled t-Test of the ratio of duration to time-to-peak between normal subjects left finger tapping and right finger tapping from images

	N	Mean	Standard Deviation
LFT	5	1.19	0.09
RFT	5	1.19	0.26

Two Sampled t-Test

DF	t-Value	Pr > |t|
8	-0.02	0.9874

Power (1-β) = 0.050

From Figure 4.2, when CP subjects were tapping with their affected hand, their duration over time-to-peak ratio was consistently less than one. A two sampled t-Test was performed, using SAS 9.1, to see if there was a significant difference between the means of the ratios for normal subjects and for CP subjects tapping with their affected hand. Since there was no significant difference between the ratio of normal subjects tapping with their right or left hand, the ratios of the right and left finger tapping were put into one group for the normal subjects. The null hypothesis was defined as no mean difference in the duration over time-to-peak ratio

between normal subjects and CP subjects tapping with their affected hand. A statistical significance level of P = 0.05, or a 95% confidence interval, was used. The results of the two sampled t-Test, shown in Table 4.4, concluded that there was a significant difference between the means of the duration over time-to-peak ratio between normal subjects and CP subjects tapping with their affected hand. The p-value was shown to be less than 0.0002.

Table 4.4 Two sampled t-Test of the ratio of duration to time-to-peak between normal subjects and CP subjects from images

	N	Mean	Standard Deviation
Normal	10	1.19	0.18
CP	5	0.60	0.25

Two Sampled t-Test

DF	t-Value	Pr > |t|
13	5.16	0.0002

Power (1-β) = 0.99

4.3 Activation Distance from the Center of the Motor Cortex

Time series images of HbO change over the detectors' field of view, located over the subjects' motor cortex (Figure 2.1), were reconstructed for every 0.05 s interval of the fNIRS measurements. Measurements at each time interval were averaged over 10 activation rest cycles prior to image reconstruction. The time-series images within the 5s to 20s time points, which represented the time interval where most of the activation occurred in a tapping-rest cycle (e.g. Figure 3.3), were averaged together to make a time-averaged image. The time-averaged images for normal subject versus cerebral palsy subjects presented different locations of activation. In order to show this difference, using a vertical line as a reference at the center of the motor cortex, we measured the distance between the reference line and the closest

activation area [60], in which the activation area was defined by the clustering algorithm in Chapter 3.3 [58], giving a thresholded image. The areas of activation were located in the thresholded image. If there was no activation area found in the ipsilateral hemisphere of tapping as defined by the thresholded image, then the largest pixel value representing the largest positive hemodynamic response in that hemisphere was used for the distance calculation. The results of this distance from center measurement is shown in Figure 4.3, where normal subjects have a black triangle and CP subjects have a white circle. The y-axis of Figure 4.3 is the ratio of the ipsilateral hemisphere of tapping distance from center over the contralateral hemisphere of tapping distance from center, and the x-axis is the distance from center of the ipsilateral hemisphere of tapping. From Figure 4.3, it can be seen that the distance from the center is consistently larger or equal for the ipsilateral hemisphere of tapping when compared to the contralateral hemisphere of tapping, in normal subjects. It can also be seen that for CP children the opposite is true, for at least left finger tapping or right finger tapping, except for Subject 10. Thus, normal subjects show a consistent pattern of having ipsilateral activation further from the center of the motor cortex, whereas cerebral palsy subjects have ipsilateral activation closer to the center of the motor cortex when tapping with either the left or right fingers.

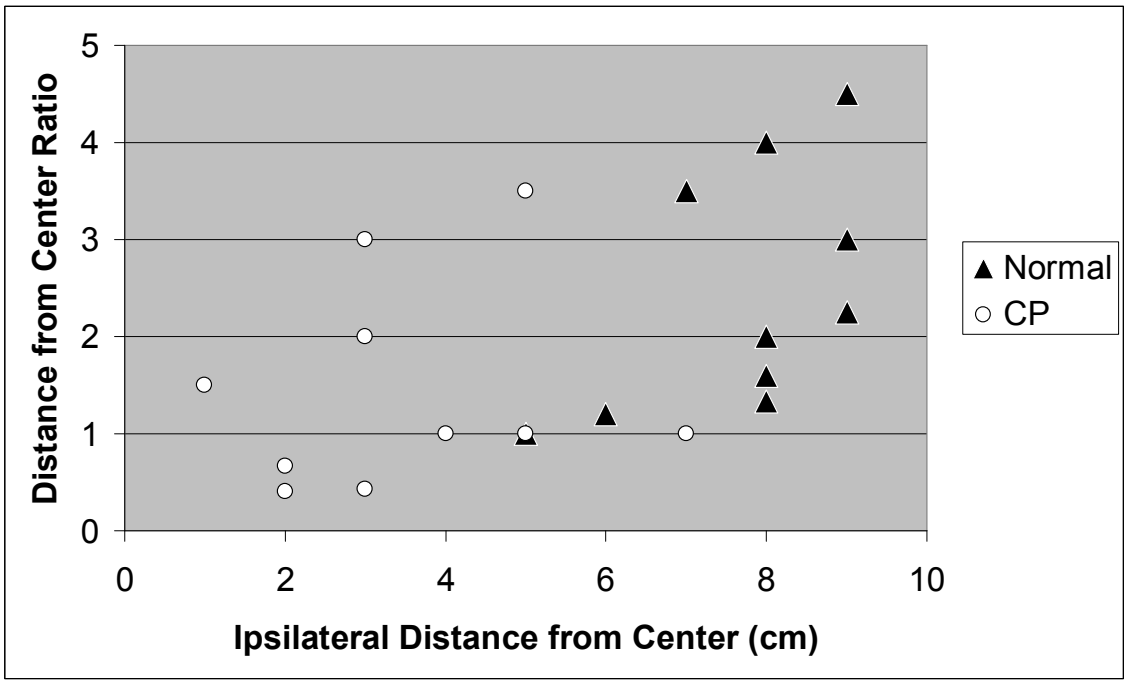

Figure 4.3 Distance from center measurements of the time-averaged images for left finger tapping and for right finger tapping of normal and CP subjects.

A two sampled t-Test was performed, using SAS 9.1, to see if there was a significant difference between the means of the distance from center metric of the ipsilateral hemisphere of tapping for normal subjects and for CP subjects. The null hypothesis was defined as no mean difference in the distance from center for the ipsilateral hemisphere of tapping. A statistical significance level of P = 0.05, or a 95% confidence interval, was used. The results of the two sampled t-Test, shown in Table 4.5, concluded that there was a significant difference between the means of the distance to center metric of the ipsilateral hemisphere of tapping between normal subjects and CP subjects. The p-value was shown to be less than 0.0001.

Table 4.5 Two sampled t-Test for distance to center of the ipsilateral hemisphere of tapping from the averaged images.

	N	Mean	Standard Deviation
Normal	10	7.70 cm	1.34 cm
CP	10	3.50 cm	1.78 cm

Two Sampled t-Test

DF	t-Value	Pr > |t|
18	5.97	<0.0001

Power (1-β) = 0.99

A two sampled t-Test was also performed, using SAS 9.1, to see if there was a significant difference between the means of the distance from center metric of the contralateral hemisphere of tapping for normal subjects and for CP subjects. The null hypothesis was defined as no mean difference in the distance from center for the contralateral hemisphere of tapping. A statistical significance level of P = 0.05, or a 95% confidence interval, was used. The results of the two sampled t-Test, shown in Table 4.6, concluded that there was no significant difference between the means of the distance to center metric of the contralateral hemisphere of tapping between normal subjects and CP subjects. The p-value was shown to be equal to 0.5402.

Table 4.6 Two sampled t-Test for distance to center of the contralateral hemisphere of tapping from the averaged images.

	N	Mean	Standard Deviation
Normal	10	3.80 cm	1.48 cm
CP	10	3.30 cm	2.06 cm

Two Sampled t-Test

DF	t-Value	Pr > |t|
18	0.62	0.5402

Power (1-β) = 0.091

4.4 Area of Activation of the Reconstructed Images

The distance from center metric gave the location of activation, but did not give the size of the activation. Since CP subjects presented activation near the center of the motor cortex, activation area was calculated within three defined areas of the motor cortex. The three defined areas of the motor cortex, shown within the time-averaged image, were the left 7 cm of the left hemisphere, the right 7 cm of the right hemisphere, and the middle 6 cm of the motor cortex, as shown in Figure 4.4. The time-averaged images were then thresholded using the same clustering algorithm used in Section 3.3 [58], giving a thresholded image. The areas of activation were located in the thresholded image. The metric of interest was the difference of activation area found between the contralateral hemisphere of tapping and the middle region of the motor cortex. The results of the area difference measurement are shown in Figure 4.5, where the bar graph patterns and labels are defined the same as in Figure 4.1. The results show that for normal subjects the area of activation in the controlateral hemisphere of tapping is always greater than the middle are of the motor cortex by at least 2 cm^2. Three of the five cerebral palsy subjects, showed greater activation area in the middle portion of the motor cortex for either left or right finger tapping. Subject 8, a right hemiparesis cerebral palsy subject,

presented a less than 1 cm^2 difference between the activation area of the contralateral hemisphere and middle areas of the motor cortex when right finger tapping. Subject 7 had similar results as the normal subjects for this metric. Overall, cerebral palsy subjects had more area of activation near the center of the motor cortex when compared to the area of activation in the contralateral hemisphere than normal subjects, for either right or left finger tapping.

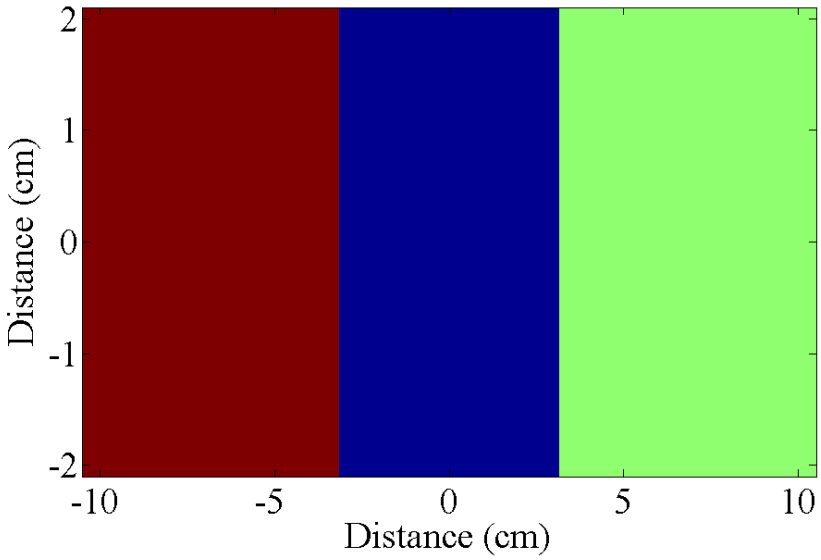

Figure 4.4 Image of the three areas measured. The red area is the left 7cm of the left hemisphere, the blue area is the middle 6cm of the motor cortex, and the green area is the right 7cm of the right hemisphere.

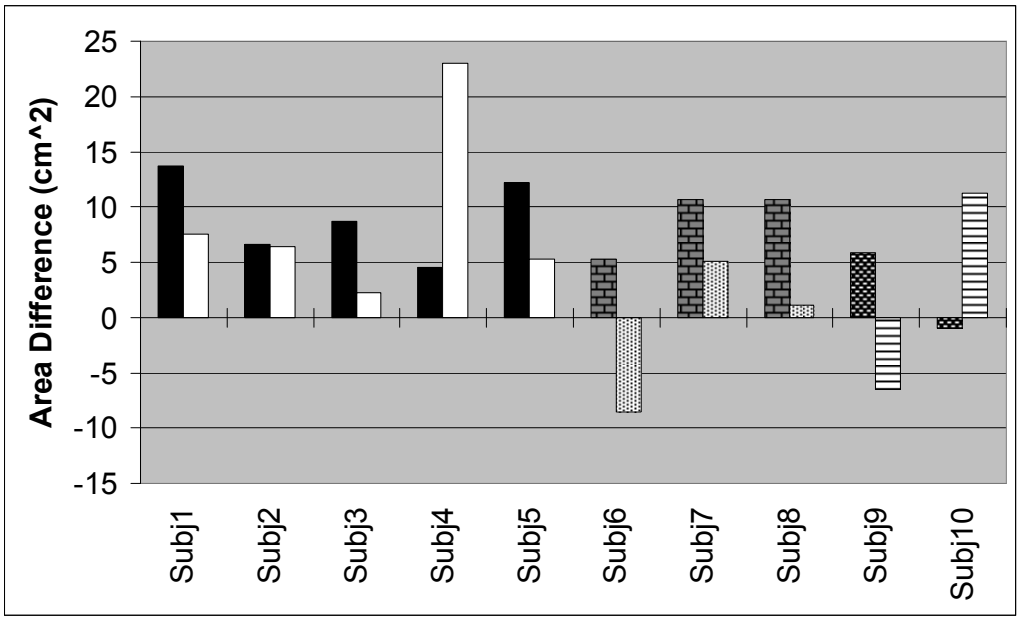

Figure 4.5 Difference of the middle area of the motor cortex to the contralateral hemisphere of tapping of the averaged images.

A two sampled t-Test was performed, using SAS 9.1, to see if there was a significant difference between the means of the area differences for normal subjects and for CP subjects tapping with their affected hand. The null hypothesis was defined as no mean difference in the area difference metric between normal and CP subjects. A statistical significance level of P = 0.05, or a 95% confidence interval, was used. The results of the two sampled t-Test, shown in Table 4.7, concluded that there was no significant difference between the means of the area difference metric for normal subjects and CP subjects. The p-value was shown to be 0.0684.

Table 4.7 Two sampled t-Test for area difference for the averaged images

	N	Mean	Standard Deviation
Normal	10	9.04 cm^2	5.96 cm^2
CP	10	3.40 cm^2	7.01 cm^2

Two Sampled t-Test

DF	t-Value	Pr > |t|
18	1.94	0.0684

Power (1-β) = 0.45

4.5 Similarity of Activation of the Reconstructed Images

When the images were reconstructed, some pixels which were not considered part of the activation area by the algorithm in Chapter 3.3 [58], showed similar temporal patterns as that of the peak activation area. In order to measure this similarity the temporal responses of each pixel were first normalized by the maximum value between its peak value and the absolute value of its minimum value. Secondly the pixels were clustered by the Euclidean distance defined by equation (4.2), where Distance is the Euclidean distance between the temporal pattern of a pixel and the mean of a cluster, pixel_value is the temporal pattern of a pixel located at an x and y coordinate on the images at a specific time point, n, and $mean_{cluster}$ is the mean vector for a specific cluster. The pixels were clustered into three groups; those similar to activation, those similar to baseline, and those similar to deactivation.

$$Distance_{cluster}(x,y) = \sum_{n=1}^{N} (pixel\_value(x,y,n) - mean(n)_{cluster})^2 \quad \textbf{(4.2)}$$

Thirdly, the curvature of the temporal signals of each pixel was measured, by calculating the angle of the temporal signal between each time point and the initial time point, which is shown in equation (4.3), theta is the angle between a the pixels zero time point and a

later time point, n [61]. The pixels were then clustered by curvature by equation (4.4), as they were clustered in the second step, where ADistance is the Euclidean distance between the vector of angles of a pixel and the mean of a cluster, pixel_angle is the curvature of a pixel located at an x and y coordinate on the images, and $Amean_{cluster}$ is the mean vector for a specific cluster. The pixels were clustered into three groups; those similar to activation, those similar to baseline, and those similar to deactivation. Each pixel was compared to the pixel with the largest amount of activation, or the seed pixel, in the second and third steps. In order for pixels to be considered similar to the seed pixel, they must be clustered with that pixel in steps two and three. The overall algorithm is presented in Figure 4.6.

$$\text{theta}(x,y,n) = \arctan(\text{pixel\_value}(x,y,n)/\text{pixel\_value}(x,y,1)) \quad \textbf{(4.3)}$$

$$\text{ADistance}_{cluster}(x,y) = \sum_{n=1}^{N} (\text{pixel\_angle}(x,y,n) - \text{Amean}(n)_{cluster})^2 \quad \textbf{(4.4)}$$

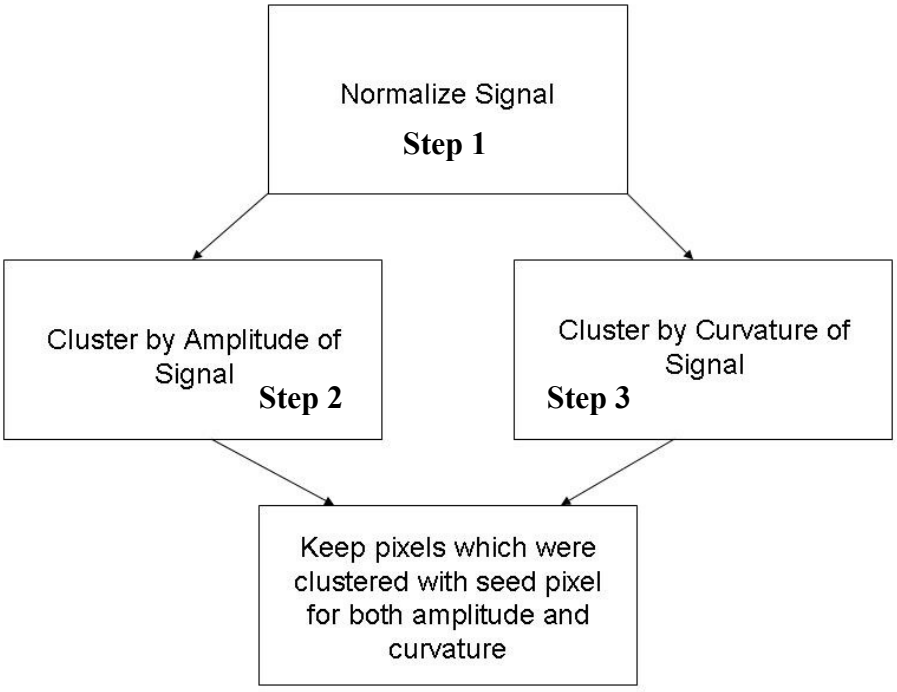

Figure 4.6 Block diagram of the similarity algorithm

By using the similarity algorithm, pixels which were considered as noise are now recognized as areas of having a hemodynamic response similar to the seed pixel. The seed pixel was determined as the pixel with the largest amount of activation. This is shown for Subject 2, a normal subject left finger tapping, in Figure 4.7, in which the white areas in Figure 4.7c are the areas which have similar hemodynamic response to the activation area (white area) shown in Figure 4.7b.

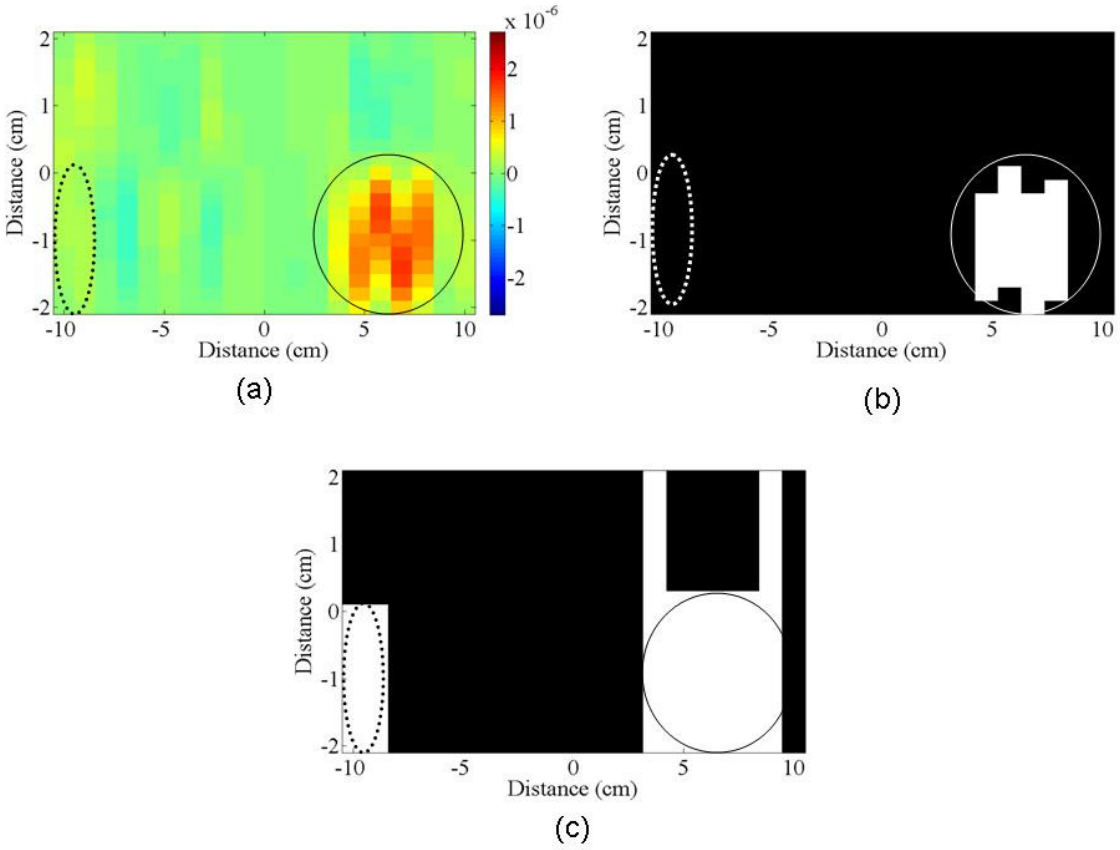

Figure 4.7 Images of a normal subject, Subject 2 left finger tapping, of (a) change in HbO concentration, (b) thresholded image showing only the area of activation, and (c) the similarity image.

Similarity between pixels and the seed pixel were also found for all the CP subjects. An example is shown in Figure 4.8 for Subject 7 left finger tapping. In Figure 4.8b, the white areas are considered as the areas of activation, whereas in Figure 4.8c the white areas are considered as areas similar to the seed pixel. As shown in the image of Figure 4.8c, similar areas are shown to be near the middle of the motor cortex as well as in the far left of the left hemisphere, while left finger tapping.

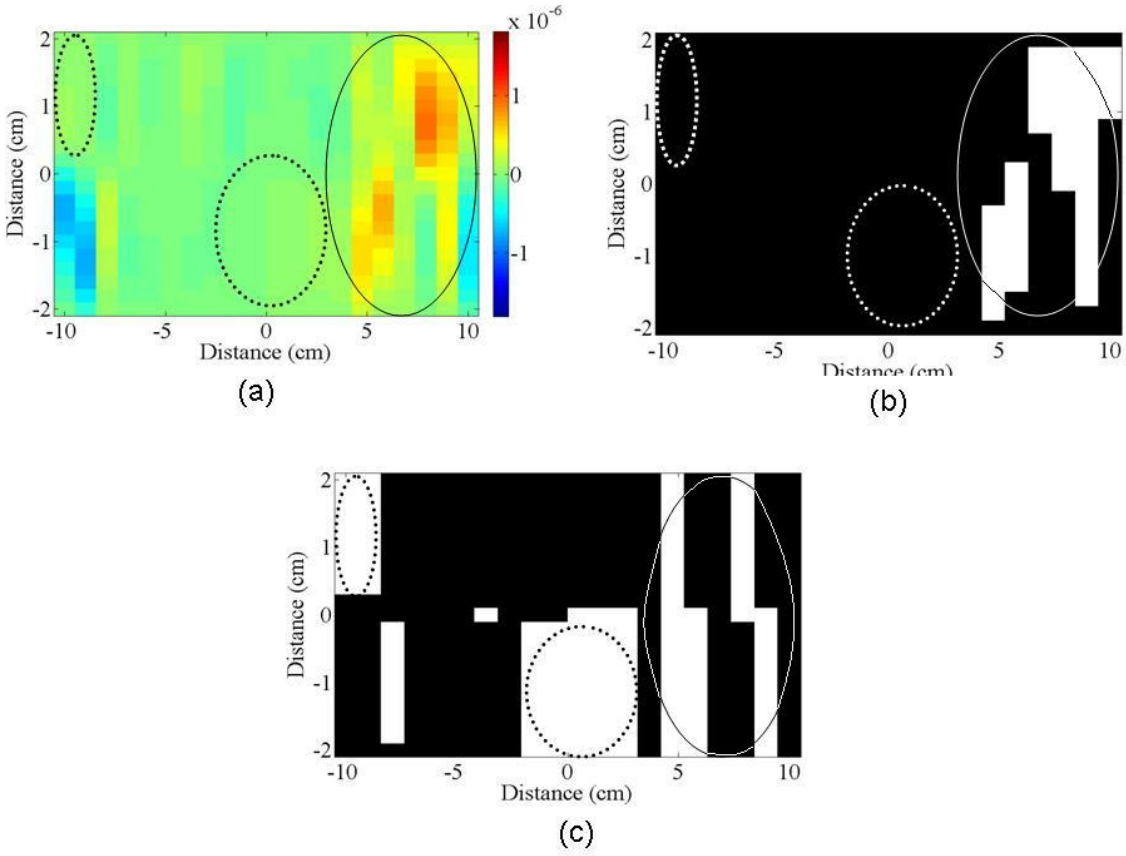

Figure 4.8 Images of a CP subject, Subject 7, of (a) change in HbO concentration, (b) thresholded image showing only the area of activation, and (c) the similarity image.

The same, distance from center and area difference, metrics were calculated for the similarity images. The distance from center results are presented in Figure 4.9, in which the subject labeling and bar patterns are the same as in Figure 4.3. From Figure 4.9, normal subjects have similar hemodynamic responses further from the center of the motor cortex than cerebral palsy children for both left and right finger tapping. Cerebral palsy children show a similar hemodynamic response to the seed pixel at the middle of the motor cortex for either left or right finger tapping, or both.

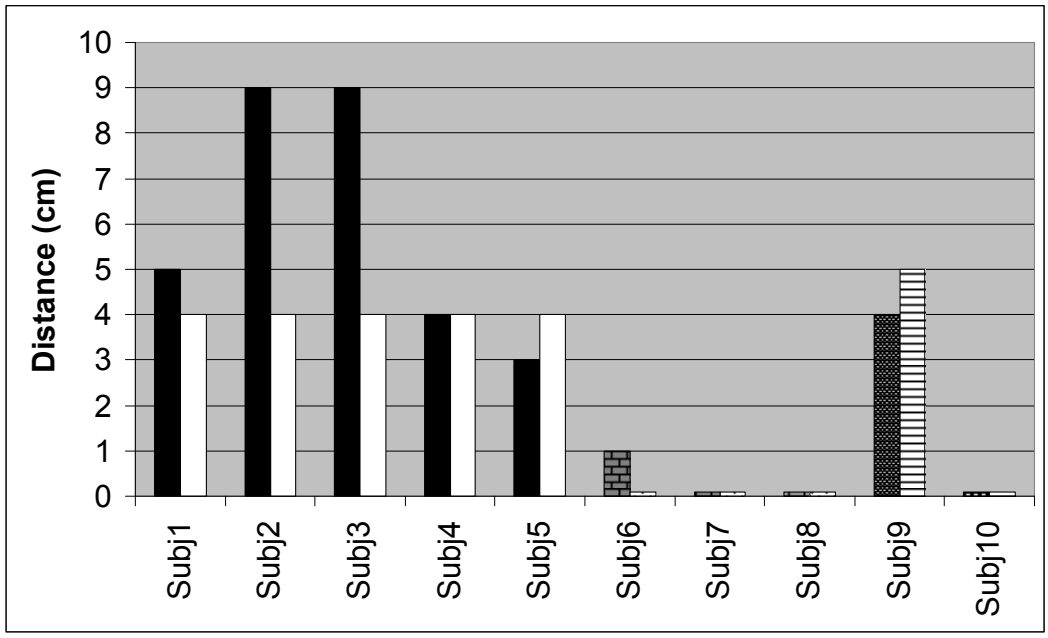

(a)

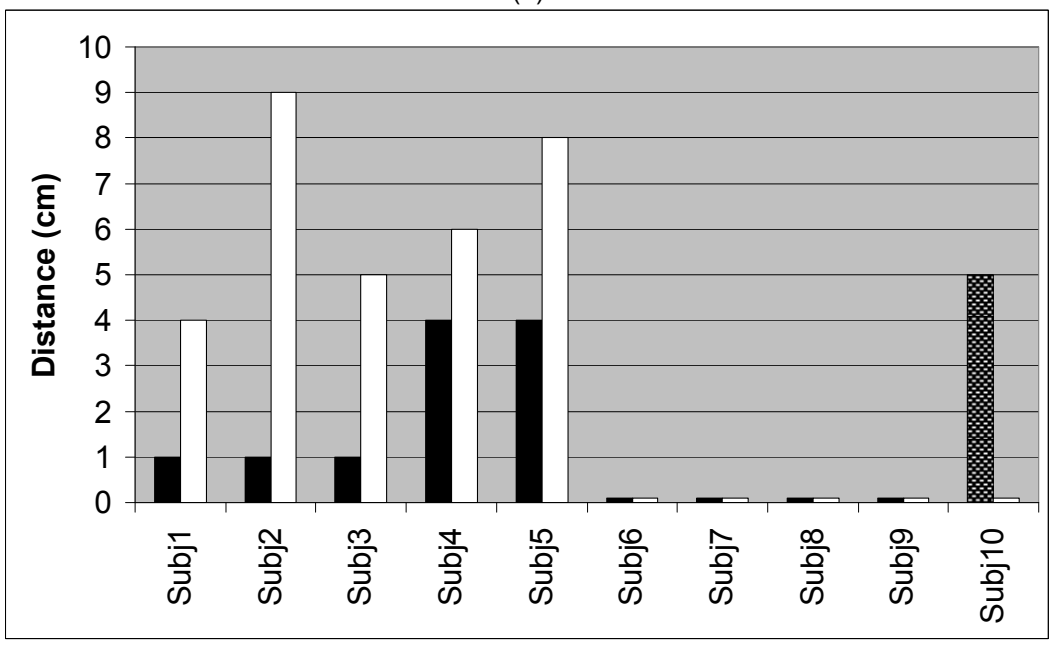

(b)

Figure 4.9 Distance from center measurements from the similarity images for (a) left finger tapping and for (b) right finger tapping.

A two sampled t-Test was performed, using SAS 9.1, to see if there was a significant difference between the means of the distance from center metric, for similarity images, of the

ipsilateral hemisphere of tapping for normal subjects and for CP subjects. The null hypothesis was defined as no mean difference in the distance from center for the ipsilateral hemisphere of tapping between normal and CP subjects. A statistical significance level of P = 0.05, or a 95% confidence interval, was used. The results of the two sampled t-Test, shown in Table 4.8, concluded that there was a significant difference between the means of the distance to center metric of the ipsilateral hemisphere of tapping between normal subjects and CP subjects. The p-value was shown to be less than 0.0001.

Table 4.8 Two sampled t-Test for distance to center for ipsilateral hemisphere of tapping from the similarity images

	N	Mean	Standard Deviation
Normal	10	6.20 cm	2.35 cm
CP	10	0.50 cm	1.27 cm

Two Sampled t-Test

DF	t-Value	Pr > |t|
18	6.75	<0.0001

Power (1-β) = 0.99

A two sampled t-Test was also performed to see if there was a significant difference between the means of the distance from center metric, for similarity images, of the contralateral hemisphere of tapping for normal subjects and for CP subjects. A statistical significance level of P = 0.05, or a 95% confidence interval, was used. The results of the two sampled t-Test, shown in Table 4.9, showed that there was a significant difference between the means of the distance to center metric of the contralateral hemisphere of tapping between normal subjects and CP subjects. The p-value was shown to be 0.0183, except the power of the analysis is 0.69. The power represents the probability that the test will correctly reject the null hypothesis when it is

false [62]. In the previous tests, the power was equal to or greater than 0.9. In order to increase the power to 0.9 for this test, four more normal and four more cerebral palsy subjects are needed, thus we cannot say there is a significant difference between the means of the distance to center metric of the contralateral hemisphere of tapping between normal subjects and CP subjects, until there are more subjects included for the study.

Table 4.9 Two sampled t-Test for distance to center for contralateral hemisphere of tapping from the similarity images.

	N	Mean	Standard Deviation
Normal	10	3.10 cm	1.45 cm
CP	10	1.00 cm	2.11 cm

Two Sampled t-Test

DF	t-Value	Pr > |t|
18	2.60	0.0183

Power (1-β) = 0.69

Area differences were also found for the similarity images. This measurement would be an area of similarity, instead of an area of activation. The area of similarity is comparing the area of similarity in the controlateral hemisphere of tapping and the center of the motor cortex. In Figure 4.10, the area of similarity on the contralateral hemisphere is always greater by at least 2 cm^2, than the area of similarity of the middle portion of the motor cortex, for normal subjects. Cerebral palsy subjects show smaller differences or greater area of similarity in the center portion of the motor cortex for either left of right finger tapping.

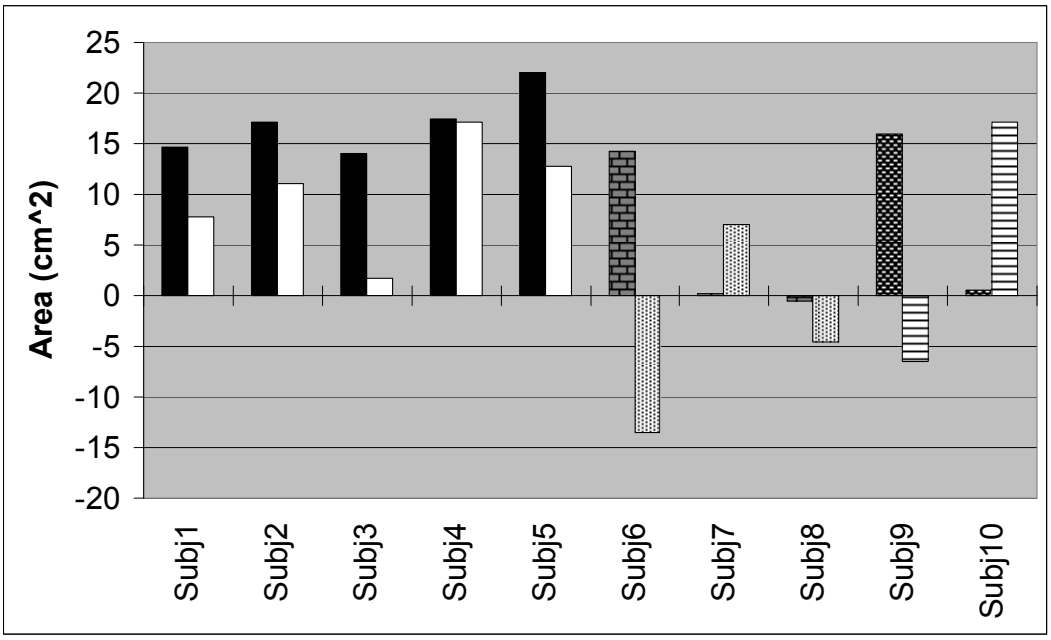

Figure 4.10 Difference of the middle area of the motor cortex to the controlateral hemisphere of tapping of the similarity images.

A two sampled t-Test was performed, using SAS 9.1, to see if there was a significant difference between the means of the area differences, of the similarity images, for normal subjects and for CP subjects tapping with their affected hand. The null hypothesis was defined as no mean difference in the area differences between normal and CP subjects. A statistical significance level of P = 0.05, or a 95% confidence interval, was used. The results of the two sampled t-Test, shown in Table 4.10, concluded that there was a significant difference between the means area differences of normal subjects and CP subjects. The p-value was shown to be 0.0110, except the power of the analysis was 0.78. The power represents the probability that the test will correctly reject the null hypothesis when it is false [62]. In the previous tests, the power was equal to or greater than 0.9. In order to increase the power to 0.9 for this test, two more normal and two more cerebral palsy subjects are needed, thus we cannot say there is a significant difference between the means of the area difference metric between normal subjects and CP subjects, until there are more subjects for the study.

Table 4.9 Two sampled t-Test for area difference from the similarity images

	N	Mean	Standard Deviation
Normal	10	13.57 cm^2	5.72 cm^2
CP	10	3.00 cm^2	10.30 cm^2

Two Sampled t-Test

DF	t-Value	Pr > |t|
18	2.84	0.0110

Power (1-β) = 0.78

CHAPTER 5

CONCLUSION AND FUTURE WORK

5.1 Conclusion

A continuous wave fNIRS instrument was used to image the HbO of the motor cortex of five normal and five CP children for a finger tapping protocol. The main sources of physiological interference were cardiac pulsation, respiration, and Mayer waves. I applied a combination of PCA and adaptive filtering to remove these artifacts. From these ten subjects an improvement in temporal SNR and CNR, and an increase in image SNR were found after filtering. The improvement of data quality was significant, leading to the conclusion that concurrent global hemodynamic signal acquisition and filtering methods may need to become standard procedure in fNIRS neuroimaging protocols. The improvement in data quality assisted in differentiating between normal and CP subjects using temporal and spatial metrics.

Since no previous study has been published on using fNIRS to assess plasticity of the motor cortex in CP children, I have identified temporal metrics from the detected reflectance signals and from the reconstructed images that show great potential for differentiating between healthy children and ones affected by cerebral palsy. In the temporal data, I found a significant difference in the ratio of the duration metric over the time-to-peak metric between normal children and CP children tapping with their affected hand. Images were then reconstructed for every 0.05 s. This same significant difference was found in the ratio of duration to time-to-peak in the temporal patterns in the activation areas of the reconstructed images.

Additionally from the reconstructed images, I identified spatial metrics with great potential for differentiating between healthy and CP children. Since the greatest amount of activation was found between 5s and 20s, images within that time were averaged together. Distance from the center and area difference metrics were found from these time-averaged

images. The distance from center metric was defined as the closest activation area to middle of the motor cortex. A significant difference of the distance from center of activation for the ipsilateral hemisphere of tapping was found between normal and CP subjects. Since CP subjects showed closer activation areas to the center of the motor cortex, the areas of activation were found for the left 7cm of the left, right 7cm of the right hemisphere, and the middle 6cm of the motor cortex. The difference between the area contralateral hemisphere of tapping and middle region of the motor cortex were found. For normal subjects, this difference was always greater than or equal to 2 cm^2. For a few CP children this difference was negative. Though there is a visual difference between subjects, no statistically significant difference was found for the area difference metric between normal and CP subjects. Different pixels of the reconstructed images, though on the images seemed to have no activation, had temporal patterns which were similar to the pixels with activation. This similarity was found by checking the normalized amplitude and curvature of temporal patterns of each pixel. The same distance from the center and area difference metrics were found for these similarity images. A significant difference of the distance from center of the similarity area for the ipsilateral hemisphere of tapping was found between normal and CP subjects. A significant difference was also found for the contralateral hemisphere, but with a power of 0.69. With 4 more normal and CP subjects, the power of the statistical test would improve to 0.9. The difference of area for the similarity images between the contralateral hemisphere of tapping and middle region of the motor cortex was found. For normal subjects, this difference was always greater than or equal to 2 cm^2. A significant difference of the area difference metric was found between normal and CP subjects, but with a power of 0.78. With 2 more normal and CP subjects, the power of the statistical test would improve.

The results of the temporal and spatial metrics identified for differentiating between normal and CP children are summarized in Table 5.1.

Table 5.1 Summary of Results of Differences between Normal and CP Subjects

Metric	p-value	Statistical Power	Additional Subjects Needed to Increase Statistical Power to 0.90	
			Normal	CP
Duration/Time-to-Peak (Detectors)	< 0.0001	0.99	0	0
Duration/Time-to-Peak (Image)	0.0002	0.99	0	0
Distance from Center (Ipsilateral Hemisphere of Reconstructed Image)	< 0.0001	0.99	0	0
Distance from Center (Ipsilateral Hemisphere of Similarity Image)	< 0.0001	0.99	0	0
Distance from Center (Contralateral Hemisphere of Similarity Image)	0.0183	0.69	4	4
Area Difference (Similarity Image)	0.0110	0.78	2	2

The presented spatial metrics show a functional reorganization of the motor cortex in CP subjects. CP subjects had areas of activation and areas of similarity closer to the center of the motor cortex than normal subjects. This would indicate that the arm or torso regions of the body are also moving while the CP subject is trying to follow the finger tapping protocol. In some cases, for areas of similarity, they may be moving to a lesser extent, since the amplitude of activation was not visibly seen in the reconstructed images. The larger area of activation and similarity near the center of the motor cortex, for CP subjects, would also indicate that the arm or torso regions of the body are moving. The epochs of tapping kept for data analysis did not have any motion artifacts in the respiration belt and pulse oximeter signals, and the video recordings did not show any additional movements within those epochs. Thus another interpretation of the resulting data may say there was no movement in the arm or torso regions,

but the healthy neurons originally responsible for the movements of those areas were used to compensate for the lack of healthy neurons in the hand region of the motor cortex. Whether there is or is not any additional muscle movement in the arm or torso regions of the body during a finger tapping task, needs to by studied in the future in CP children.

5.2 Future Work

The results presented here are part of a subject population that will grow in the future as we are currently recruiting more healthy volunteer children as well as ones affected by cerebral palsy. We plan to apply our developed filtering methods to this subject population and assess differences in the detected fNIRS temporal and spatial activation patterns between the two subject groups.

For the filtering approach presented in this work the hemodynamic reference signals from the pulse oximeter and respiration belt were acquired at anatomical locations that were distant from the locations where detectors were placed on the scalp. Even though time delays between reference and activation signals were corrected for by our cross-correlation approach, the hemodynamic profiles for cardiac pulsation and respiration may not have been identical to those measured at the respective distal locations. In the future, mapping the respiratory delay as a function of detector position may help in understanding the propagation of respiratory noise through the scalp. A better approach may be to apply our proposed filtering method to a reference signal obtained from fNIRS measurements on the surface of the scalp. More specifically, small source detector separations result in NIR light traveling only superficially and therefore mostly sample scalp hemodynamics, but not the deeper cortical activation kinetics [15], [17]. In future work we could add detector channels at short source-detector separations to sample the local scalp hemodynamics and adaptively filter them out of the underlying cortical activation signals. This may be carried out in conjunction with the hemodynamic measurements.

Since no fNIRS studies on CP children have been published to our knowledge, we should compare results with fMRI by having concurrent fMRI and fNIRS measurements. The concurrent measurements will help validate fNIRS findings since fMRI is considered the “gold standard”. fNIRS measurements should also be extended to more severe hemiplegic and quadriplegic CP patients. In order to get clearer differences in the future, splitting the research into right hemiparetic CP subjects versus normal subjects, and left hemiparetic CP subjects versus normal subjects may give valuable results. The metrics presented in this study can potentially be used as biomarkers to assess plasticity in CP subjects undergoing treatment. These metrics can then be correlated with current CP classification schemes, such as MACS and SHUEE. The fNIRS metrics can help identify the effectiveness of the therapy, and help identify physiological improvement in CP patients. Further efforts can be done in order to subtype CP patients by fNIRS metrics in order to improve the sensitivity of current CP classification schemes.

In order to better understand the physiological meaning behind the spatial metrics presented in this paper, additional EMGs should be placed on the upper arms and torso. This would help validate if the CP subjects are using additional muscles to compensate for their difficulty in tapping. If no additional muscles are used during finger tapping, then the neurons in those healthy regions of the brain are being used to compensate for the damaged area.

Future work should also include finding differences in tapping using a tapping board and EMGs. Instead of finding the peak activation from the when the subject was told to tap, there is a potential of quantifying the time delay between the start of tapping and the peak activation by using the tapping board as a reference for tapping. Since CP subjects had more difficulty tapping, differences in tapping frequency and quantifying tapping efficiency between normal and CP subjects may also be found. Correlations between the hemodynamic response and EMG or tapping board signals, may give additional insight on the physical motion and brain activity.

APPENDIX A

CW-5 SPECIFICATIONS

CW5 Specifications

Transmitters: Laser Sources

Number of sources.....24
Type of source.....Laser
Source wavelengths.....690 and 830 nm
Optical Output
Power per source..... 9 mW, 3 mW
Output control
Capability modulation.....On/Off, Square-wave
Connector type.....Optical SMA

Receivers: Detectors

Number of receivers..... 24
Type of receiver..... Avalanche Photo Diode
Photo sensitivity..... 0.5 A/W @ 800 nm
Gain Range..... -12 To +84 dB
Optical bandwidth..... 400-1000 nm
Signal bandwidth..... 16 kHz
Control capability..... On/Off &
programmable Gain
Connector type..... Optical SMA

External Remote Control Details:

Electrical Interface..... Serial
Control Language..... Proprietary
Data bit rate..... 5 kHz

General Physical Details (approximate as shown in photograph):

Input power.....10V AC 60 Hz @ 2.5A
Operating Temperature.....0 to 40 C
Storage Temperature.....-20 to 60 _C
Humidity..... 5 to 95 %
noncondensing
Dimensions with.....Length 20 inches
Enclosure Width 20 inches
Height 17 inches
Rack Mountable 19 “width
Weight..... 100lbs in enclosure

APPENDIX B

CODE FOR FILTERING, TEMPORAL METRICS, AND SPATIAL METRICS

CODE FOR PCA FILTER

```
function [H_clean] = PCA(Hstim, Hbase, eigen_number)
%%INPUTS
% Hstim is the time data. It has all 28 source-detector pairs
% Hbase is the first 30s of baseline data for all 28 source-detector
pairs
% eigen_number is the number of eigenvectors being considered to be
noise



% m = number of times points
% n = number of source-detector pairs
[m, n] = size(Hbase);

% Cbase is covariance matrix of the first 30s of baseline data
Cbase = (1/m)*Hbase'*Hbase;

% Do the eigen decomposition of the covariance matrix
[Ubase, Sigbase] = eig(Cbase);

% Keep the eigenvector that is related to noise
Ubaser = Ubase(:,1:eigen_number);
[m, n] = size(Ubaser);
I = eye([m m]);

% Clean the rest of the signal
H_clean = (I - Ubaser*Ubaser')*Hstim';
H_clean = H_clean';

return
```

CODE FOR DELAY CORRECTION

```
function [NIRS_R_pad, Resp_pad] = Resp_Padding(NIRS_R, Resp,Lag)

%% INPUTS:
% NIRS_R is the NIRS signal filtered for the respiration frequencies
% Resp is the respiration belt signal
% Lag is the amount of lag found by cross-correlation

%% OUTPUTS:
% NIRS_R_pad is the NIRS signal returned
% Resp_pad is the padded respiration noise reference signal

if Lag > 0
    Padding_Sig = zeros(Lag,1);
    NIRS_R_pad = cat(1,NIRS_R,Padding_Sig);
    R_Noise_pad = zeros(Lag,1);
    Resp_pad = cat(1,R_Noise_pad,Resp);
end
if Lag < 0
    Padding_Sig = zeros(abs(Lag),1);
    NIRS_R_pad = cat(1,Padding_Sig,NIRS_R);
    R_Noise_pad = zeros(abs(Lag),1);
    Resp_pad = cat(1,Resp,R_Noise_pad);
end
if Lag == 0
    NIRS_R_pad = NIRS_R;
    Resp_pad = Resp;
end

return
```

CODE FOR ADAPTIVELY FILTERING RESPIRATION

```
function [filtsignal,e] = AdaptiveFilterResp(NoisySignal, Noise, Lag)
% INPUTS:
% NoisySignal = the signal that needs filtering
% Noise = the reference noise measured
% Lag = the amount of Lag found by cross-correlation

% OUTPUTS:
% filtsignal = adaptively filtered signal
% e = error of filter

L = 600;          % Number of weights in filter
mu = 0.0001;      % Step size mu
%mu = 0.0001;
%mu = 0.0005;     % seems to work best, but cancels to much of signal

%Initialize LMS filter
%h = adaptfilt.lms(L,mu,1,coeff);

%Need to go through every source-detector pair individually for
adaptive
%filter algorithm to work properly
[row,column] = size(NoisySignal);
colcount = 1;
while colcount < column + 1
    %First normalize each signal
    NSignal(:,colcount) = NoisySignal(:,colcount) /
std(NoisySignal(:,colcount));
    NSignal(:,colcount) = NSignal(:,colcount) -
mean(NSignal(:,colcount));
    N(:,colcount) = Noise / std(Noise);
    N(:,colcount) = N(:,colcount) - mean(N(:,colcount));
    % GET INITIAL WEIGHTS


    %[y,e] = thisfilter(this,x,d);
    [Mn,Nn] = size(N(1:600,colcount));
    [Mns,Nns] = size(NSignal(1:600,colcount));

    %  Variable initialization
    h = adaptfilt.lms(L,mu); % Works Well
    msg = checkfilterinputs(h,[Mn,Nn],[Mns,Nns]);
    error(msg);
    [ntr,L,e,f,X,W,mu,lam] = initlmsfiltering(h,[Mn,Nn]);
%    W(1) = 1;
    [W,X] =
InitialWeights(ntr,L,e,f,X,W,mu,lam,N(1:600,colcount),NSignal(1:600,co
lcount));
    savestates(h,W,X,ntr,L);
```

```
    %DO ACTUAL ADAPTIVE FILTERING
    %[y,e] = thisfilter(this,x,d);
    [Mn,Nn] = size(N(:,colcount));
    [Mns,Nns] = size(NSignal(:,colcount));
    msg = checkfilterinputs(h,[Mn,Nn],[Mns,Nns]);
    error(msg);

    %  Variable initialization
    [ntr,L,e,filtsignal(:,colcount),X,W,mu,lam] =
initlmsfiltering(h,[Mn,Nn]);

    %  Main loop
    for n=1:ntr,
        X(2:L) = X(1:L-1);   %shift temporary input signal buffer down
        X(1) = N(n,colcount);    %  assign current input signal sample
        e(n,colcount) = W*X;     %  compute and assign current output
signal sample
        filtsignal(n,colcount) = NSignal(n,colcount) - e(n);     %
compute and assign current error signal sample
        W = lam*W + mu*filtsignal(n,colcount)*X'; %  update filter
coefficient vector
    end

    %  Save States
    savestates(h,W,X,ntr,L);
    %Multiply back the standard deviation to retrieve proper scaling
    filtsignal(:,colcount) =
filtsignal(:,colcount)*std(NoisySignal(:,colcount));
    e(:,colcount) = e(:,colcount)*std(NoisySignal(:,colcount));

    clear h
    colcount = colcount + 1;
end
if Lag > 0
    filtsignal = filtsignal(1:end-Lag,:);
    e = e(1:end-Lag,:);
end
if Lag < 0
    filtsignal = filtsignal(abs(Lag)+1:end,:);
    e = e(abs(Lag)+1:end,:);
end
return
```

CODE FOR ADAPTIVELY FILTERING CARDIAC PULSATION

```
function [filtsignal,e] = AdaptiveFilterCard(NoisySignal, Noise)
% INPUTS:
% NoisySignal = the signal that needs filtering
% Noise = the reference noise measured

% OUTPUTS:
% filtsignal = adaptively filtered signal
% e = error of filter

%fs = 20.0318 Hz

% Number of weights in filter
L = 100;

% Step size mu
mu = 0.0003;

%Initialize LMS filter
%h = adaptfilt.lms(L,mu,1,coeff);

%Need to go through every source-detector pair individually for
adaptive
%filter algorithm to work properly
[row,column] = size(NoisySignal);
colcount = 1;
while colcount < column + 1
    %First normalize each signal
    NSignal(:,colcount) = NoisySignal(:,colcount) /
std(NoisySignal(:,colcount));
    NSignal(:,colcount) = NSignal(:,colcount) -
mean(NSignal(:,colcount));
    N(:,colcount) = Noise / std(Noise);
    N(:,colcount) = N(:,colcount) - mean(N(:,colcount));
    % GET INITIAL WEIGHTS


    %[y,e] = thisfilter(this,x,d);
    [Mn,Nn] = size(N(1:600,colcount));
    [Mns,Nns] = size(NSignal(1:600,colcount));

    %  Variable initialization
    h = adaptfilt.lms(L,mu); % Works Well
    msg = checkfilterinputs(h,[Mn,Nn],[Mns,Nns]);
    error(msg);
    [ntr,L,e,f,X,W,mu,lam] = initlmsfiltering(h,[Mn,Nn]);
    %W(1) = 1;
```

```
    [W,X] =
InitialWeights(ntr,L,e,f,X,W,mu,lam,N(1:600,colcount),NSignal(1:600,co
lcount));
    savestates(h,W,X,ntr,L);


    %DO ACTUAL ADAPTIVE FILTERING

    %[y,e] = thisfilter(this,x,d);
    [Mn,Nn] = size(N(:,colcount));
    [Mns,Nns] = size(NSignal(:,colcount));
    msg = checkfilterinputs(h,[Mn,Nn],[Mns,Nns]);
    error(msg);

    %  Variable initialization
    [ntr,L,e,filtsignal(:,colcount),X,W,mu,lam] =
initlmsfiltering(h,[Mn,Nn]);

    %  Main loop

    for n=1:ntr,
        X(2:L) = X(1:L-1);      %  shift temporary input signal buffer
down
        X(1) = N(n,colcount);            %  assign current input
signal sample
        e(n,colcount) = W*X;             %  compute and assign current
output signal sample
        filtsignal(n,colcount) = NSignal(n,colcount) - e(n);     %
compute and assign current error signal sample
        W = lam*W + mu*filtsignal(n,colcount)*X'; %  update filter
coefficient vector
    end

    %  Save States
    savestates(h,W,X,ntr,L);

    %Multiply back the standard deviation to retrieve proper scaling
    filtsignal(:,colcount) =
filtsignal(:,colcount)*std(NoisySignal(:,colcount));
    e(:,colcount) = e(:,colcount)*std(NoisySignal(:,colcount));

    clear h
    colcount = colcount + 1;
end

return
```

CODE TO CALCULATE DURATION

```
function [Duration_HbO] = Thresh_Dur(dataSave,thresh_HbO,fs)
%%INPUTS
% dataSave is the temporal signals from the detectors
% thresh_HbO is the threshold value for finding the duration
% fs is the sampling frequency

%%OUTPUTS
% Duration_HbO is the duration of each channel
 [row, column] = size(dataSave);

% Get spatio-temporal plot of the channels
Left_HbO = dataSave(:,1:column/2);
Right_HbO = dataSave(:,(column/2 + 1):end);

Left_HbO = Left_HbO';
Right_HbO = flipud(Right_HbO');

Image_HbO = cat(1, Left_HbO, Right_HbO);
% Image_HbO = Image_HbO';

% Threshold image
BWHbO = Image_HbO > thresh_HbO;
Combo_HbO = Image_HbO .* BWHbO;

% Calculate duration for each channel
cnt = 1;
while cnt < column + 1
    Duration_HbO(cnt) = sum(BWHbO(cnt,1:end))*(1/fs);
    cnt = cnt + 1;
end
Duration_HbO = Duration_HbO';

return
```

CODE TO CALCULATE TIME-TO-PEAK

```
function [RiseTimeL] = TimetoPeak(dataSave)
%PURPOSE: Calculate the time to peak for the averaged signals
%INPUT:
%------
%Averaged signal

%OUTPUT:
%-------
%Time to peak for each source-detector pair
sdpair = 1;
[row, column] = size(dataSave(:,:));
while sdpair < column + 1
    % Find all max and mins
    [maxx, minn] = peakdet(dataSave(1:end,sdpair), 0.01e-5);
    % Find only peak
    HbOBig = max(maxx(:,2));
    HbOBigt = 0;
    n = 1;
    s = size(maxx);
    % Find when that peak happened
    while n < s(1) + 1
        if maxx(n,2) == HbOBig
            HbOBigt = maxx(n,1);
        end
        n = n + 1;
    end
    % Convert from samples to time. Sampling frequency is 20Hz
    RiseTimeL(sdpair) = HbOBigt*.05;
    sdpair = sdpair + 1;
end
RiseTimeL = RiseTimeL';
return
```

CODE TO CLUSTER FOR IMAGE SNR

```
function [Cluster1, Cluster2, Cluster3] = kMeansCluster(Image)
% Find time it takes to run through algorithm
tic

%%INPUTS:
% Image = Image being clustered

%%OUTPUTS:
% Cluster1 = activation cluster
% Cluster2 = noise cluster
% Cluster3 = deactivation cluster

%% Initialize Cluster
Length_Image = length(Image(:));
Image = Image(:);

Cluster1 = max(Image(:));
Cluster2 = 0;
Cluster3 = min(Image(:));

%% Cluster Image
% [I_num, I_val] = hist(Image(:), Length_Image);
it = 1; % number of iterations
d1 = 0;
d2 = 0;
d3 = 0;
mean1 = Cluster1(1);
mean2 = Cluster2(1);
mean3 = Cluster3(1);
while 1
% while it < Nit + 1
    cnt = 1;
    cnt1 = 1;
    cnt2 = 1;
    cnt3 = 1;

    % Reinitialize clusters
    if it >= 2
        Cluster1 = 0;
        Cluster2 = 0;
        Cluster3 = 0;
    end

    while cnt < Length_Image + 1
        % Calculate Euclidean Distances
        d1 = Euclidean_Distance(Image(cnt), mean1);
        d2 = Euclidean_Distance(Image(cnt), mean2);
        d3 = Euclidean_Distance(Image(cnt), mean3);
```

```
        % Find the minimum distance
        min1 = min(d1,d2);
        mindistance = min(min1,d3);

        % Place into proper cluster
        if (mindistance == d1) && (mindistance ~= d2) && (mindistance
~= d3)
            Cluster1(cnt1) = Image(cnt);
            cnt1 = cnt1 + 1;
        end
        if (mindistance == d2) && (mindistance ~= d1) && (mindistance
~= d3)
            Cluster2(cnt2) = Image(cnt);
            cnt2 = cnt2 + 1;
        end
        if (mindistance == d3) && (mindistance ~= d1) && (mindistance
~= d2)
            Cluster3(cnt3) = Image(cnt);
            cnt3 = cnt3 + 1;
        end
        if (mindistance == d1) && (mindistance == d2) && (mindistance
~= d3)
            Cluster1(cnt1) = Image(cnt);
            cnt1 = cnt1 + 1;
        end
        if (mindistance == d2) && (mindistance == d3) && (mindistance
~= d1)
            Cluster2(cnt2) = Image(cnt);
            cnt2 = cnt2 + 1;
        end
        if (mindistance == d1) && (mindistance == d2) && (mindistance
== d3)
            Cluster1(cnt1) = Image(cnt);
            cnt1 = cnt1 + 1;
        end
        cnt = cnt + 1;
    end
    % Recalculate means of each cluster
    mean1_old = mean1;
    mean2_old = mean2;
    mean3_old = mean3;
    mean1 = mean(Cluster1);
    mean2 = mean(Cluster2);
    mean3 = mean(Cluster3);

    % If the means of each cluster is not changing, then break the
loop.
    if (mean1_old == mean1) && (mean2_old == mean2) && (mean3_old ==
mean3)
        break;
```

```
    end

    % Save previous clusters
    Cluster1_old = Cluster1;
    Cluster2_old = Cluster2;
    Cluster3_old = Cluster3;

    % Go through another iteration
    it = it + 1;
end
t = toc;
return
```

CODE TO CALCULATE IMAGE AREA

```
function [Left_Area, Right_Area] = Image_Area(Image)
%% INPUTS
% Image = Thresholded Averaged Image

%% OUTPUTS
% Left_Area = area found for left 7cm of left hemisphere
% Right_Area = area found for right 7cm of right hemisphere
Left_Image = Image(:,1:7);
Right_Image = Image(:,14:20);

Left_Area = sum(Left_Image(:));
Right_Area = sum(Right_Image(:));

return

function [Marea] = Middle_Area(BW)
%% INPUTS
% BW = Thresholded Averaged Image

%% OUPUTS
% Marea = area in middle 6cm of motor cortex
Marea = sum(BW(:,8:13));
Marea = sum(Marea);

return
```

CODE TO CALCULATE SIMILARITY OF AMPLITUDE AND SIMILARITY BY CURVATURE

```
function [Similar] = Similarity_Distance(Sig1,Sig2)
%% INPUTS
% Sig1 = seed pixel normalized temporal pattern
% Sig2 = other pixel normalized temporal pattern

%% OUTPUTS
% Similar = difference between Sig1 and Sig2

Sig1 = Sig1(:);
Sig2 = Sig2(:);

% N = length(Sig1);

% Find difference in amplitude
Similar = (Sig1 - Sig2).^2;
Similar = Similar(:);

return

function [ds1,angle1] = SAM(Sig1)
%% INPUTS
% Sig1 = pixel normalized temporal pattern

%% OUTPUTS
% ds1 = arclength
% angle1 = angle
Sig1 = Sig1(:);
N = length(Sig1);

for n=1:N
    if n == 1
        angle1(n) = 0;
        mag(n) = Sig1(n);
        ds1(n) = 0;
    else
        mag(n) = Sig1(n) - mag(1);
        angle1(n) = atand(mag(n));
        R = sqrt((n-1)^2 + mag(n)^2);
        ds1(n) = 2*pi*R*angle1(n)/360;
    end
end

return
```

CODE TO CLUSTER TO GET SIMILARITY IMAGES

```
function [Cluster1, Cluster2, Cluster3,it] = kMeansCluster2Dmet(Image)
% Check amount of time algorithm takes
tic

%%INPUTS
% Image = Reconstructed Images at every 0.05s (It is a 3D array)

%% OUTPUTS
% Cluster1 = Those similar to seed pixel
% Cluster2 = Those similar to noise
% Cluster3 = Those similar to deactivation

%% Initialize Cluster Vectors

avgImage = mean(Image,3);
m = max(avgImage(:));
small = min(avgImage(:));
[row,column,time] = size(Image);

rcnt = 1;
while rcnt < row + 1
    colcnt = 1;
    while colcnt < column + 1
        if avgImage(rcnt,colcnt) == m
            mrow = rcnt;
            mcol = colcnt;
        end
        if avgImage(rcnt,colcnt) == small
            srow = rcnt;
            scol = colcnt;
        end
        colcnt = colcnt + 1;
    end
    rcnt = rcnt + 1;
end

% [I_num, I_val] = hist(Image(:), Length_Image);
it = 1;
d1 = 0;
d2 = 0;
d3 = 0;
mean1 = Image(mrow,mcol,:);
mean1 = mean1(:);
mean2 = zeros(length(mean1(:)),1);
mean3 = Image(srow,scol,:);
mean3 = mean3(:);

if mean(mean3) == mean(mean2)
```

```
        mean2 = Image(mrow-1,mcol-1,:);
        mean2 = mean2(:);
end

%% Cluster Image
while 1
% while it < Nit + 1
    cnt = 1;
    cnt1 = 1;
    cnt2 = 1;
    cnt3 = 1;

    % Reinitialize clusters
    if it >= 2
        clear Cluster1 Cluster2 Cluster3
    end
    for rcnt = 1:row
        for colcnt=1:column
            % Calculate Euclidean Distances
            d1 = Euclidean_Distance2D(Image(rcnt,colcnt,:), mean1);
            d2 = Euclidean_Distance2D(Image(rcnt,colcnt,:), mean2);
            d3 = Euclidean_Distance2D(Image(rcnt,colcnt,:), mean3);

            % Find the minimum distance
            min1 = min(d1,d2);
            mindistance = min(min1,d3);

            % Place into proper cluster
            if (mindistance == d1) && (mindistance ~= d2) &&
(mindistance ~= d3)
                I = Image(rcnt,colcnt,:);
                Cluster1(:,cnt1) = I(:);
                cnt1 = cnt1 + 1;
            end
            if (mindistance == d2) && (mindistance ~= d1) &&
(mindistance ~= d3)
                I = Image(rcnt,colcnt,:);
                Cluster2(:,cnt2) = I(:);
                cnt2 = cnt2 + 1;
            end
            if (mindistance == d3) && (mindistance ~= d1) &&
(mindistance ~= d2)
                I = Image(rcnt,colcnt,:);
                Cluster3(:,cnt3) = I(:);
                cnt3 = cnt3 + 1;
            end
            if (mindistance == d1) && (mindistance == d2) &&
(mindistance ~= d3)
                I = Image(rcnt,colcnt,:);
                Cluster1(:,cnt1) = I(:);
                cnt1 = cnt1 + 1;
```

```
            end
            if (mindistance == d2) && (mindistance == d3) &&
(mindistance ~= d1)
                I = Image(rcnt,colcnt,:);
                Cluster2(:,cnt2) = I(:);
                cnt2 = cnt2 + 1;
            end
            if (mindistance == d1) && (mindistance == d2) &&
(mindistance == d3)
                I = Image(rcnt,colcnt,:);
                Cluster1(:,cnt1) = I(:);
                cnt1 = cnt1 + 1;
            end
        end
    end
    % Recalculate means of each cluster
    mean1_old = mean1;
    mean2_old = mean2;
    mean3_old = mean3;
    mean1 = mean(Cluster1,2);
    mean2 = mean(Cluster2,2);
    if ~exist('Cluster3','var')
        mean3 = 1000;
        break
    else
        mean3 = mean(Cluster3,2);
        Cluster3_old = Cluster3;
    end

    % If the means of each cluster is not changing, then break the
loop.
    if (mean(mean1_old) == mean(mean1)) && (mean(mean2_old) ==
mean(mean2)) && (mean(mean3_old) == mean(mean3))
        break;
    end
%     if it == 6
%         break;
%     end

    % Save previous clusters
    Cluster1_old = Cluster1;
    Cluster2_old = Cluster2;

    % Go through another iteration
    it = it + 1;
end
if mean3 == 1000
    Cluster3 = ones(length(mean1(:)),1);
end
t = toc;
return
```

REFERENCES

[1] S. Bunce, M. Izzetoglu, K. Izzetoglu, B. Onaral, and K. Pourrezaei, "Functional Near-Infrared Spectroscopy," *IEEE Engineering in Medicine and Biology Magazine*, pp. 54-61, 2006.

[2] D. Boas, A. Dale, and M. Franceschini, "Diffuse optical imaging of brain activation: approaches to optimizing image sensitivity, resolution, and accuracy," *Neuroimage*, vol. 23, pp. S275-S288, 2004.

[3] A.P. Gibson, J.C. Hebden, and S.R. Arridge, "Recent advances in diffuse optical imaging," *Phys. Med. Biol.*, vol. 50, pp. R1-R43, 2005.

[4] M. Franceschini, S. Fantini, J. Thompson, J. Culver, D. Boas, "Hemodynamic evoked response of the sensorimotor cortex measured noninvasively with near-infrared optical imaging," *Pyschophysiology*, vol. 40, pp. 548-560, 2003.

[5] M. Schweiger, J. Gibson, and S.R. Arridge, "Computational aspects of diffuse optical tomography," *IEEE.*, vol. 3, pp. 1521-9615, 2003.

[6] B. Chance, M. Cope, E. Gratton, N. Ramanujam, and B. Tromberg, "Phase measurement of light absorption and scatter in human tissue," *Review of Scientific Instruments*, vol. 69(10), pp. 3457-3481, 1998.

[7] M. Cope and D.T. Delpy, “System for long-term measurement of cerebral blood flow and tissue oxygenation on newborn infants by infra-red transillumination,” *Med. Biol. Eng. Comput.*, vol. 26, pp. 289-294, 1988.

[8] B. Chance, Z. Zhuang, C. Unah, C. Alter, and L. Lipton, "Cognition-activated low-frequency modulation of light absorption in human brain," *Proc. Natl. Acad. Sci. USA*, vol. 90, pp. 3770-3774, 1993.

[9] R. B. Buxton, "The elusive initial dip," *NeuroImage*, vol. 13, pp. 953-958, 2001.

[10] P.T. Fox and M. E. Raichle, M. A. Mintum, and C. Dence, "Nonoxidative glucose consumption during focal physiologic neural activity," *Science*, vol. 241, pp. 462-464, 1988.

[11] A. Villringer and B. Chance, “Non-invasive optical spectroscopy and imaging of human brain function,” *Trends Neurosci.*, vol. 20, pp. 435–442, 1997.

[12] H. Girouard and C. Iadecola, “Neurovascular coupling in the normal brain in hypertension, stroke, and Alzheimer disease,” *J. Appl. Physiol.*, vol. 100, pp. 328-335, 2006.

[13] J. Filosa and V. Blanco, “Neurovascular coupling in the mammalian brain,” *Exp. Physiol.*, vol. 92.4, pp. 641-646, 2007.

[14] K. Paemeleire, “The cellular basis of neurovascular metabolic coupling,” *Acta neurol. Belg.*, vol. 102, pp. 153-157, 2002.

[15] S. Vannucci, F. Maher, I. Simpson, "Glucose transporter proteins in brain: delivery of glucose to neurons and glia," *Glia*, vol. 21, pp. 2-21, 1997.

[16] E. E. Benarroch, "Neuron-astrocyte interactions: partnership for normal function and disease in the central nervous system," *Mayo Clin. Proc.*, vol. 80(10), pp. 1326-1338, 2005.

[17] P. J. Magistretti and L. Pellerin, "Cellular mechanisms of brain energy metabolism and their relevance to functional brain imaging," *Phil. Trans. R. Soc. Lond.*, vol. 354, pp. 1155-1163, 1999.

[18] P. T. Fox and M. E. Raichle, "Focal physiological uncoupling of cerebral blood flow and oxidative metabolism during somatosensory stimulation in human subjects," *Proc. Natl. Acad. Sci. USA*, vol. 83, pp. 1140-1144, 1986.

[19] R. Cooper, H. J. Crow, W. G. Walter, and A. L. Winter, "Regional control of cerebral vascular reactivity and oxygen in man," *Brain Research*, vol. 3, pp. 174-191, 1966.

[20] R. C. Koehler, R. J. Roman, and D. R. Harder, "Astrocytes and the regulation of cerebral blood flow," *Trends in Neuroscience*, vol. 32(3), pp. 160-167, 2008.

[21] P. Somogyi, B. Tamas, R. Lujan, and E. H. Buhl, "Salient features of synaptic organisation in the cerebral cortex," *Brain Research Reviews*, vol. 26, pp.113-135, 1998.

[22] www.scholarpedia.org/wiki/image/3/33/PasleyNV1.jpg

[23] J. N. Sanes and J. P. Donoghue, "Plasticity and primary motor cortex," *Annu. Rev. Neurosci.*, vol. 23, pp. 393-415, 2000.

[24] www.marketoracle.co.uk/images/dorn_4_11_07b.jpg

[25] www.thetutoradvantage.com/images/homunculus.jpg

[26] R. D. Kent, J. R. Duffy, A. Slama, J.F. Kent, and A. Clift, "Clinicoanatomic studies in Dysarthria: review, critique, and directions for research," *Journal of Speech, Language, and Hearing Research*, vol. 44, pp. 535-551. 2001.

[27] www.iupucanatomy.com/images/picture1188.jpg

[28] T. Sato, M. Ito, T. Suto, M. Kameyama, M. Suda, Y. Yamagishi, A. Ohshima, T. Uehara, M. Fukuda, and M. Mikuni, "Time courses of brain activation and their implications for function: A multichannel near-infrared spectroscopy study during finger tapping," *Neuroscience Research*, vol. 58, pp. 297-304, 2007.

[29] C. Julien, "The enigma of Mayer waves: Facts and models," *Cardiovascular Research*, vol. 70, pp 12-21, 2006.

[30] Y. Zhang, D. Brooks, M. Franceschini, and D. Boas, "Eigenvector-based spatial filtering for reduction of physiological interference in diffuse optical imaging," *Journal of Biomedical Optics*, vol. 10(1), pp. 1-11, 2005.

[31] Q. Zhang, E. Brown, and G. Strangman, "Adaptive filtering for global interference cancellation and real-time recovery of evoked brain activity: a Monte Carlo simulation," *Journal of Biomedical Optics*, vol. 12(4), pp. 1-12, 2007.

[32] G. Morren, M. Wolf, P. Lemmerling, U. Wolf, J.H. Choi, E. Gratton, L. De Lethauwer, and S. Van Huffel, "Detection of fast neural signals in the motor cortex from function near infrared spectroscopy measurements using independent component analysis," *Med. Biol. Eng. Comput.*, vol. 42, pp. 92-99, 2004.

[33] F. Tian, S. Prajapati, and H. Liu, "A Location-Adaptive, Frequency-Specific Cancellation Algorithm to Improve Optical Brain Functional Imaging," *Biomedical Optics*, vol. BMD29, 2008.

[34] A. F. Abdelnour and T. Huppert, "Real-time imaging of human brain function by near-infrared spectroscopy using an adaptive general linear model," *NeuroImage*, to be published.

[35] http://children.webmd.com/tc/cerebral-palsy-topic-overview

[36] W. Kulak, W. Sobaniec, J. Kuzia, and L. Bockowski, “Neurophysiologic and neuroimaging studies of brain plasticity in children with spastic cerebral palsy,” *Exp. Neurology*, vol. 198, pp. 4-11, 20006.

[37] L.J. Carr et al. “Patterns of central motor reorganization in hemiplegic cerebral palsy,” *Brain*, vol. 116, pp. 1223-1247, 1993.

[38] Y. Maegaki et al., “Central motor reorganization in cerebral palsy patients with bilateral cerebral lesions,” *Pediatr. Res.*, vol. 45, pp. 559-567, 1999.

[39] G.W. Thickbroom et al., “Differences in sensory and motor cortical organization following brain injury early in life,” *Ann. Neurol.*, vol. 49, pp. 320-327. 2001.

[40] M. Staudt et al., “Two types of ipsilateral reorganization in congenital hemiparesis. A TMS and fMRI study,” *Brain*, vol. 125, pp. 2222-2237, 2002.

[41] Y. Vandermereen, M. Davare, J. Duque, and E. Olivier, “Reorganization of cortical hand representation in congenital hemiplegia,” *European Journal of Neuroscience*, vol. 29, pp. 845-854, 2009.

[42] Y. Vandermereen et al., “Functional reorganization of brain in children affected with congenital hemiplegia: fMRI study,” *Neuroimage*, vol. 20, pp. 289-301, 2003.

[43] W. Kulak and W. Sobaniec, “Quantitative EEG analysis in children with hemiparetic cerebral palsy,” *NeuroRehabilitation*, vol. 20, pp. 75-84, 2005.

[44] J. Detre and J. Wang, "Technical aspects and utility of fMRI using BOLD and ASL," *Clinical Neurophysiology*, vol. 113, pp. 621-634, 2002.

[45] F. Di Salle, E. Formisano, D.E.J. Linden, R. Goebel, S. Bonavita, A. Pepino, F. Smaltino, and G. Tedeschi, "Exploring brain function with magnetic resonance imaging," *European Journal of Radiology*, vol. 30, pp. 84-94, 1999.

[46] M. Wilke, S. K. Holland, J. S. Myseros, V. J. Schmithorst, and W. S. Ball, "Functional magnetic resonance imaging in pediatrics," *Neuropediatrics,* vol. 34(5), p. 225-233, 2003.

[47] A. Eliasson et al., “The manual ability classification system (MACS) for children with cerebral palsy: scale development and evidence of validity and reliability,” *Development Medicine and Child Neurology*, vol. 48, pp. 549-554, 2006.

[48] J. Davis et al., “Validation of the shriners hospital for children upper extremity evaluation (SHUEE) for children with hemiplegic cerebral palsy,” *The Journal of Bone and Joint Surgery*, vol. 88-A, pp. 326-333, 2006.

[49] R.W. Bohannon and M.B. Smith, “Interrater reliability of a modified Ashworth scale of muscle spasticity,” *Phys. Ther.*, vol. 67, pp. 206-207, 1987.

[50] J.H. House, F.W. Gwathmey, and M.O. Fidler, “A dynamic approach to the thumb in palm deformity in cerebral palsy,” *J. Bone Joint Surg. Am.*, vol. 63, pp. 216-225, 1981.

[51] G. Strangman, M. Fraceschini, and D. Boas, "Factors affecting the accuracy of near-infrared spectroscopy concentrations for focal changes in oxygenation parameters," *NeuroImage*, vol. 18, pp. 865-879. 2003.

[52] T.J. Huppert and D.A. Boas (2005, July 28), "HOMER: Hemodynamic evoked response NIRS data analysis GUI"[Online]. Available: http://www.nmr.mgh.harvard.edu/PMI

[53] M. Kilmer, P. C. Hansen, M. I. Espanol, "A projection-based approach to general-form Tikhonov regularization," SIAM J. Sci. Comput., vol. 29, No. 1, pp. 315-330, 2007.

[54] J. Wang, "Recurrent neural networks for computing pseudoinverses of rank-deficient matrices," SIAM J. Sci. Comput., vol. 18, No. 5, pp. 1479-1493, 1997.

[55] V.K. Ingle and J.G. Proakis, "Digital Signal Processing using Matlab," 2nd ed., Pacific Grove, CA: Brooks/Cole, 2000, pp. 27-29.

[56] S.M. Kuo, B.H. Lee, and W. Tian, "Real-Time Digital Signal Processing: Implementations and Applications," Hoboken, NJ: John Wiley and Sons Ltd., 2006, pp. 354-364.

[57] G. Proakis and D.G. Manolakis, "Digital Signal Processing: Principles, Algorithms, and Applications," 4th ed., Saddle River, NJ: Prentice Hall, 2007, pp. 975-985.

[58] K. Fukunaga, *Statistical Pattern Recognition*, 2nd ed., Academic Press, 1990.

[59] J. MacQueen. "Some Methods for Classification and Analysis of Multivariate Observations," Proc. 5th Berkeley Symp. on Math. Stat. Prob., p.281, 1967.

[60] N. Asanini, “Study of NIRS based motor cortex activation patterns in cerebral palsy affected kids using image based metrics,” University of Texas at Arlington, Arlington, Texas, 2008.

[61] T. Sebastian, P. Klein, and B. Kimia, “On Aligning Curves,” *IEEE Transactions on Pattern Analysis and Machine Intelligence*, vol. 25, pp. 116-124. 2003.

[62] J. H. Zar, "Biostastical Analysis," 3nd ed., Upper Saddle River, NJ: Prentice Hall, 1996, pp. 65-178.

BIOGRAPHICAL INFORMATION

Bilal Khan was born in Wichita, Kansas, on March 4, 1984. He received his Bachelors of Science in Electrical Engineering from the University of Texas at Austin in May of 2007. In the fall of 2006 he began his graduate studies in biomedical engineering from the joint program of biomedical engineering at the University of Texas at Arlington and the University of Texas Southwestern Medical Center at Dallas. His research has been in signal processing, bioinstrumentation, and optical imaging. He plans to further his education by pursuing a PhD degree in biomedical engineering.